


# Monitoring Postharvest Ethylene Emissions in Fresh Produce: Potential of Metal Oxide Semiconductor-Based Gas Sensors

Cheyeon Kim<sup>1</sup>, Sang-Won Lee<sup>1</sup>, Junha Hwang<sup>1</sup>, and Ji-Wook Yoon<sup>1,\*</sup>

<sup>1</sup>Department of Information Materials Engineering, Division of Advanced Materials Engineering, Jeonbuk National University, Jeonju 54896, Republic of Korea.

 Cite This: *J. Sens. Sci. Technol.* Vol. 34, No. 2 (2025) 138-157

 <https://doi.org/10.46670/JSST.2025.34.2.138>

**ABSTRACT:** Ethylene is a key plant hormone that regulates the ripening and senescence of fresh produce. Although it is essential for maturation, its presence also accelerates deterioration, leading to quality loss and food waste. Real-time ethylene monitoring is crucial for optimizing postharvest management and extending shelf life in storage and distribution networks. Among the various gas sensing technologies, metal oxide semiconductor (MOS)-based sensors have emerged as a promising solution owing to their high response, simple structure, and cost-effectiveness. However, detecting ethylene in complex postharvest environments remains challenging because of its low reactivity and cross-sensitivity to interfering gases. This review explores advancements in modern ethylene sensor technologies, with a particular focus on MOS-based ethylene sensors. Key strategies for enhancing sensor response and selectivity are examined, including nanostructuring, catalyst decoration, composite material development, and bilayer film fabrication. Additionally, the integration of sensor arrays and machine learning techniques for precise real-time ethylene detection is discussed. By addressing existing challenges and recent innovations, this review provides valuable insights into MOS-based ethylene sensing and offers guidance for the development of next-generation sensors. These advancements hold significant potential for improving postharvest management, reducing food waste, and enhancing supply chain efficiency in fresh produce distribution networks.

**KEYWORDS:** *Postharvest Monitoring, Ethylene Sensing, Metal Oxide Semiconductor Sensors, Response Enhancement, Selectivity Enhancement*

## 1. INTRODUCTION

Ethylene is a key plant hormone that regulates the ripening and senescence of fresh produce. Although it plays a crucial role in fruit maturation and flavor development, its presence also accelerates quality deterioration, leading to softening, discoloration, and physiological disorders [1]. Even trace amounts of ethylene can induce undesirable ripening and spoilage, posing significant challenges to postharvest management. Given the global reliance on efficient food distribution networks, monitoring and controlling ethylene emissions are essential for preserving produce quality and minimizing food waste.

Recent advancements in gas sensor technologies have

enabled real-time ethylene detection [2], providing a proactive approach to mitigating its negative effects. Among the various sensing platforms, metal oxide semiconductor (MOS)-based sensors have emerged as a promising solution owing to their high response, simple structure, and cost-effectiveness [3-6]. However, detecting ethylene in postharvest environments remains challenging because of its low reactivity and the presence of volatile organic compounds (VOCs) such as ethanol and acetaldehyde, which can interfere with ethylene sensing [7]. Therefore, addressing these limitations by improving ethylene response and selectivity has become a central focus in MOS sensor research.

This review examines the latest advancements in MOS-based ethylene sensors, focusing on strategies to enhance ethylene response and selectivity. Section 2.1 discusses ethylene emissions from fresh produce and their impact on postharvest quality, emphasizing the need for effective ethylene monitoring. Section 2.2 examines the advantages and limitations of various ethylene sensor technologies, including optical, piezoelectric, electrochemical, and chemiresistive sensors, while emphasizing the potential of MOS sensors as a promising

\*Corresponding author: [jwyoona@jbnu.ac.kr](mailto:jwyoona@jbnu.ac.kr)

Received : Feb. 12, 2025, Accepted : Feb. 13, 2025

This is an Open Access article distributed under the terms of the Creative Commons Attribution Non-Commercial License (<https://creativecommons.org/licenses/by-nc/3.0/>) which permits unrestricted non-commercial use, distribution, and reproduction in any medium, provided the original work is properly cited.

**Table 1.** Classification of postharvest commodities based on ethylene emission rates [13-27].

Class	Ethylene emission rate ( $\mu\text{L}\cdot\text{kg}^{-1}\cdot\text{h}^{-1}$ )	Commodities	Post-exposure symptoms	Respiration type	Ref.
Very low	< 0.1	Cherry	Shrinking	Non-climacteric	[13]
		Broccoli	Yellowing		[14]
		Asparagus	Toughening		[15]
Low	0.1 – 1.0	Cucumber	Yellowing		[16]
		Green pepper	Decay		[17]
		Watermelon	Water-soaking		[18]
Moderate	1.0 – 10	Banana	Decay	[19]	
		Tomato	Shrinking, decay	[20]	
		Mango	Decay	[21]	
High	10 – 100	Apple	Scalding, losing crunch	Climacteric	[22]
		Avocado	Decay		[23]
		Pear	Decay		[24]
Very high	> 100	Mammee apple	Scalding, losing crunch		[25]
		Passion fruit	Decay		[26]
		Cherimoya	Browning		[27]

alternative for enhancing ethylene detection. Section 2.3 provides an in-depth analysis of MOS sensors for ethylene detection, covering gas-sensing mechanisms and advanced strategies such as nanostructure design, catalyst decoration, composite material development, and bilayer film fabrication to enhance sensor response and selectivity. Additionally, we discuss sensor array configurations and the integration of machine learning techniques for precise real-time ethylene monitoring in complex gas environments. Finally, we outline future research directions, identifying key challenges and opportunities for next-generation ethylene sensors. This review provides valuable insights and new opportunities for researchers and industries seeking to enhance postharvest management and reduce global food losses.

## 2. BODY

### 2.1 Postharvest Ethylene Emissions and Their Impacts on Fresh Produce

Ethylene is a natural plant hormone that regulates key physiological processes, particularly fruit ripening and senescence [1]. It is continuously produced throughout plant growth and remains active after harvesting, influencing various physiological processes.

Ethylene is a colorless and flammable gas with a slightly sweet odor [8]. Its molecular weight is 28.05 g/mol, and its specific gravity is 0.97. Because of its high diffusivity, ethylene spreads rapidly in open spaces [9]. However, it can accu-

mulate in enclosed environments such as warehouses, cargo containers, and refrigerated trucks, thereby significantly affecting the quality of fresh produce. Moreover, ethylene can react with other compounds or undergo oxidation, altering storage conditions and ripening processes [10].

The rate of ethylene emission varies depending on several factors, including biological characteristics (*e.g.*, type of produce and maturity level), environmental conditions (*e.g.*, temperature and vapor pressure), and postharvest handling (*e.g.*, storage duration and chemical treatments) [11]. Nevertheless, according to Kader [12], fresh produce can be categorized into five classes based on ethylene emission levels after harvest:

- Very high ( $>100 \mu\text{L}\cdot\text{kg}^{-1}\cdot\text{h}^{-1}$ )
- High ( $10\text{--}100 \mu\text{L}\cdot\text{kg}^{-1}\cdot\text{h}^{-1}$ )
- Moderate ( $1.0\text{--}10 \mu\text{L}\cdot\text{kg}^{-1}\cdot\text{h}^{-1}$ )
- Low ( $0.1\text{--}1.0 \mu\text{L}\cdot\text{kg}^{-1}\cdot\text{h}^{-1}$ )
- Very low ( $<0.1 \mu\text{L}\cdot\text{kg}^{-1}\cdot\text{h}^{-1}$ )

Representative fruits, listed in decreasing order of ethylene emissions, include passion fruits (very high), apples (high), bananas (moderate), watermelons (low), and cherries (very low). A detailed classification of fruits and vegetables based on ethylene emission levels is presented in Table 1.

A more widely used classification system categorizes fruits and vegetables as either climacteric or non-climacteric based on their ripening behavior and response to ethylene.

Although this classification does not perfectly correspond to the above ethylene emission levels, produce with very low ethylene emissions is generally classified as non-climacteric,

whereas produce with moderate or higher ethylene emissions is typically climacteric. Fruits and vegetables with low ethylene emissions may fall into either category, depending on their specific species and physiological characteristics (Table 1).

Climacteric produce undergoes a significant increase in respiration rate and ethylene production during ripening. This self-sustained ethylene production promotes further ripening, even after harvesting. As a result, these fruits and vegetables can be harvested unripe and later ripened naturally or artificially via ethylene exposure [28]. However, as ripening progresses to senescence, ethylene accelerates deterioration, leading to decay, softening, discoloration (*e.g.*, browning), and the development of unpleasant odors. For example, apples, which release high to very high levels of ethylene ( $>10 \mu\text{L}\cdot\text{kg}^{-1}\cdot\text{h}^{-1}$ ), undergo rapid softening when exposed to high ethylene concentrations (1100 ppm), leading to a 1.85-fold decrease in firmness compared to unexposed apples [22]. Similarly, bananas and tomatoes, which emit intermediate levels of ethylene ( $1.0\text{--}10 \mu\text{L}\cdot\text{kg}^{-1}\cdot\text{h}^{-1}$ ), undergo accelerated decay and discoloration upon ethylene exposure [12,19]. Other climacteric fruits, such as mangoes and peaches, exhibit similar deterioration [21,29], resulting in a rapid decline in quality during distribution.

Non-climacteric produce does not undergo a significant increase in respiration or ethylene production after harvesting. These fruits and vegetables must fully ripen on the plant, as they do not continue to ripen or develop additional sweetness once picked. Representative examples include strawberries, potatoes, broccoli, and oranges. Despite their low ethylene production, non-climacteric produce may still experience quality deterioration, including shrinking, texture changes, and discoloration, when exposed to ethylene. For instance, cherries, which emit less than  $0.1 \mu\text{L}\cdot\text{kg}^{-1}\cdot\text{h}^{-1}$  of ethylene, can shrink rapidly when exposed to 10 ppm ethylene for 21 days [13]. Similarly, cucumbers, despite having a low emission rate ( $0.1\text{--}1.0 \mu\text{L}\cdot\text{kg}^{-1}\cdot\text{h}^{-1}$ ), exhibit accelerated yellowing under continuous exposure to 10 ppm ethylene [16]. These examples highlight the need for careful ethylene management throughout the distribution network to preserve the quality of fresh produce, regardless of its climacteric or non-climacteric classification.

Wills *et al.* [30] investigated the importance of ethylene management through a controlled study on 30 types of fresh produce. They established controlled storage environments by injecting 5 ppb or 100 ppb of ethylene into chambers containing fresh produce and monitored the changes in quality and spoilage behavior. Their findings revealed that fresh produce stored at ethylene concentrations below 5 ppb exhibited an average shelf-life extension of 62% across the tested produce types. Notably, broccoli stored at concentrations below 5 ppb demonstrated a storage extension of 20 days, whereas lettuce exhibited a storage extension of 23 days.

These results indicate that minimizing ethylene levels can slow quality deterioration in fresh produce, highlighting the urgent need for effective ethylene management to extend shelf life. Ethylene sensors capable of monitoring trace ethylene concentrations throughout a distribution network are required to achieve this goal.

## 2.2 Ethylene Sensor Technologies: Advances, Challenges, and Future Directions

### 2.2.1 Optical, Piezoelectric, and Electrochemical Sensors

Several analytical techniques have been utilized for ethylene detection in fresh produce, including gas chromatography-flame ionization detection [31-33], proton-transfer reaction mass spectrometry [34,35], selective reagent ionization mass spectrometry [36], Fourier-transform infrared spectroscopy [37,38], and photoacoustic spectroscopy [39-41]. Although these methods offer high sensitivity and accuracy, they are limited by their high cost, operational complexity, and requirements for specialized data analysis. These constraints restrict their feasibility for real-time ethylene monitoring and field applications in fresh produce distribution networks.

Compared to traditional analytical techniques, sensor-based technologies offer advantages such as compact size, cost-effectiveness, ease of operation, and real-time monitoring capabilities. However, for practical applications, ethylene sensors must exhibit high sensitivity, selectivity, cost efficiency, and structural simplicity while maintaining a broad detection range and mechanical stability under variable environmental conditions. Modern ethylene sensors can be broadly classified as optical, piezoelectric, electrochemical, and chemiresistive sensors, each of which has distinct advantages and limitations.

#### *Optical Sensors*

Optical sensors detect ethylene by analyzing its interaction with light through absorption, emission, or scattering at specific wavelengths. Raman spectroscopy [42] and surface-enhanced Raman spectroscopy [43] detect ethylene via inelastic scattering, providing high molecular specificity and low detection limits. Fluorescence- and chemiluminescence-based sensors [44,45] exploit the emission changes induced by ethylene interactions, enabling highly sensitive and selective detection. Despite their potential, making these technologies viable for practical field applications will require cost reduction, miniaturization, and the development of continuous monitoring capabilities.

Non-dispersive infrared (NDIR) sensors overcome several limitations of other optical sensor types, making them more suitable for real-world applications. An NDIR sensor consists of an IR light source, a gas sample chamber, an optical filter,

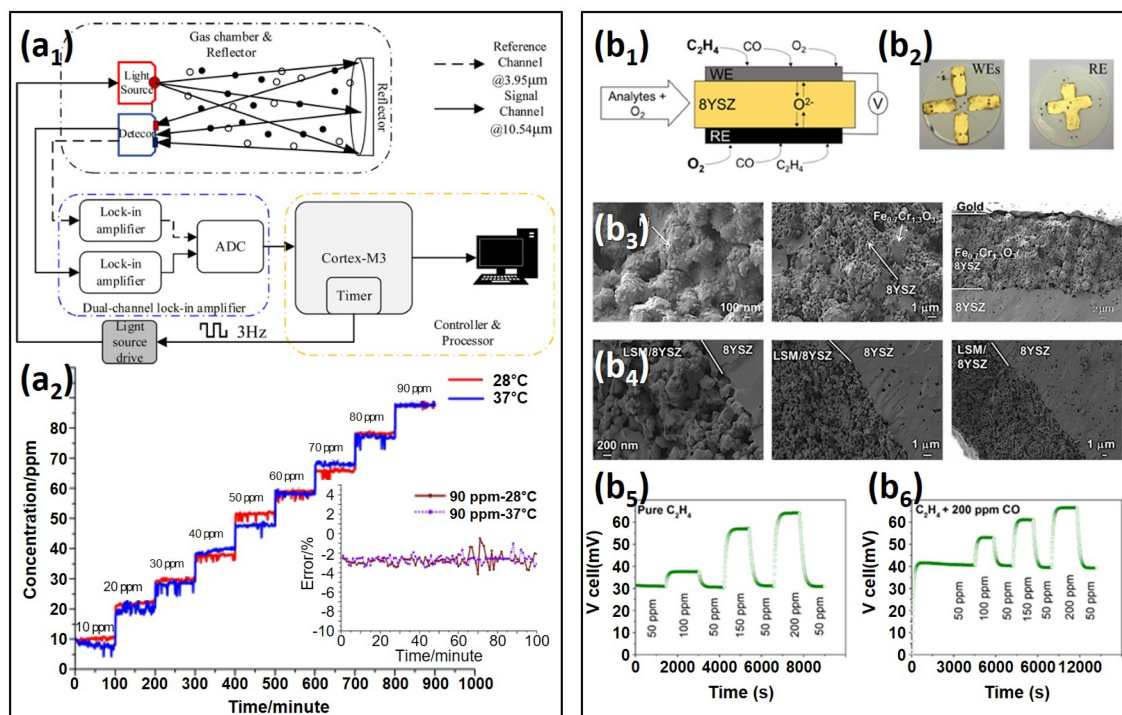


**Fig. 1.** Optical and electrochemical ethylene sensors: (a) NDIR sensor: (a<sub>1</sub>) Block diagram of the sensor system and (a<sub>2</sub>) concentration measurement curves at two different temperatures. The inset figure displays the error curve over time for a 90 ppm gas input. Reproduced with permission [48]. Copyright 2020, Elsevier. (b) Electrochemical sensor: (b<sub>1</sub>) Cross-sectional schematic of the sensor device, illustrating the reactions occurring at each electrode. (b<sub>2</sub>) Top view of the sensor, showing four Fe<sub>0.7</sub>Cr<sub>1.3</sub>O<sub>3</sub>/8YSZ electrodes (channels) with individual gold layers serving as current collectors. (b<sub>3</sub>) Scanning electron microscopy (SEM) image of the device cross-section at the Fe<sub>0.7</sub>Cr<sub>1.3</sub>O<sub>3</sub>/8YSZ working electrode (WE). (b<sub>4</sub>) SEM image of the cross-section at the LSM/8YSZ reference electrode (RE). (b<sub>5</sub>) Response curves to varying ethylene (C<sub>2</sub>H<sub>4</sub>) concentrations. (b<sub>6</sub>) Response curves for C<sub>2</sub>H<sub>4</sub> detection in the presence of a 200 ppm CO background. Reproduced with permission [57]. Copyright 2018, ACS.

and an IR detector [46]. As IR light passes through the ethylene-containing chamber, specific wavelengths around 10.6  $\mu\text{m}$  are absorbed due to ethylene's characteristic absorption bands, enabling selective and accurate detection. However, the sensitivity of NDIR sensors is constrained by high reflection losses, weak ethylene absorption, and external interference such as background noise and light scattering.

To enhance NDIR sensitivity, research has focused on sensor design optimization. Kathirvelan *et al.* [47] introduced key innovations in IR emission source tuning, detector selection, and optical path design, significantly improving ethylene detection performance. A thermal IR emission source precisely tuned to ethylene's absorption wavelength, was applied to replace conventional broadband IR sources, ensuring stronger absorption and a higher measurable signal. The integration of a high-sensitivity silicon temperature detector enhanced thermal response and signal stability, addressing the low signal-to-noise ratio (SNR) of traditional thermopile detectors. An optimized optical path extended the ethylene interaction length without increasing the sensor size, while advanced signal processing minimized background noise and improved accuracy.

These advancements significantly improved in ethylene sensitivity, achieving 3.3% ppm<sup>-1</sup> sensitivity and a detection limit of 5 ppm.

Further improvements were made by Zhang *et al.* [48], who developed a high-sensitivity NDIR ethylene sensor incorporating a dual-channel lock-in amplifier (Fig. 1 (a)). The dual-channel lock-in amplifier significantly improved the SNR to 52 dB, enabling the detection of weak ethylene signals. Other innovations included an optimized IR light path, advanced signal processing, and temperature compensation techniques. A high-efficiency reflective gas cell increased the optical path length while maintaining a compact design, achieving an IR light collection efficiency of 92%. A dual-wavelength differential method was used, with 10.54  $\mu\text{m}$  for ethylene absorption and 3.95  $\mu\text{m}$  as a reference, enhancing selectivity. In addition, a dual-temperature compensation method stabilized the sensor response, minimizing drift and improving accuracy. Consequently, the sensor achieved a detection limit close to 1 ppm, with less than 10% relative error across ethylene concentrations of 1–100 ppm.

Despite these advancements, NDIR sensors remain insuf-

**Table 2.** Comparison of ethylene-sensing performance of NDIR, QCM, and electrochemical sensors [59-70].

Sensing type	Ethylene conc. (ppm)	Sensitivity	Detection range (ppm)	Detection limit (ppm)	Ref.
NDIR	100	4.2 (%)	0 – 100	25	[59]
NDIR	100	50 (dB)	0 – 100	2	[60]
NDIR	100	-	0 – 400	30	[61]
NDIR	50	7.17 ( $\mu$ V)	0 – 50	20	[62]
NDIR	20	4.31 (V)	0 – 100	20	[63]
QCM	50	255 (Hz)	2 – 100	0.27	[64]
QCM	1000	51 (Hz)	3 – 600	3	[65]
Electrochemical	10	1	0 – 10	0.04	[66]
Electrochemical	1	9 ( $\mu$ V)	0 – 100	0.1	[67]
Electrochemical	200	40 (mV)	0 – 200	-	[68]
Electrochemical	1	9.6	0.01 – 10	0.01	[69]
Electrochemical	100	188 (mV)	0 – 100	-	[70]

efficient for detecting trace levels of ethylene in fresh produce distribution networks. Although complex structural modifications and advanced components could enhance sensitivity, they compromise cost-effectiveness, miniaturization, and mechanical stability, limiting their practical applicability. Future research should focus on enhancing ethylene absorption and minimizing signal interference to further improve reliability and accuracy while preserving high sensitivity and structural simplicity.

#### Piezoelectric Sensors

Piezoelectric sensors detect ethylene by measuring frequency shifts induced by mass variations in sensing films deposited on piezoelectric substrates [49,50]. Among these, quartz crystal microbalance (QCM) sensors have been the most widely studied because of their simple structure, high sensitivity, frequency stability, and functional versatility [51].

Kristine and Tolentino [52] investigated a QCM sensor incorporating an  $\text{AgBF}_4$ -polyvinylpyrrolidone (PVP) composite as the sensing film. The sensor's vibration frequency remained at 9.994 MHz in the absence of a sensing film. When a PVP coating was applied, the sensor frequency remained unchanged upon ethylene exposure, indicating minimal interaction between PVP and ethylene. In contrast, the  $\text{AgBF}_4$  coating resulted in a slight decrease in the frequency, suggesting ethylene adsorption via interactions with the  $\text{Ag}^+$  ions in  $\text{AgBF}_4$ . Upon introducing the  $\text{AgBF}_4$ -PVP composite, the frequency decreased significantly to 9.979 MHz, which was attributed to the enhanced separation of  $\text{Ag}^+$  from its anion by the oxygen atom in PVP, improving its accessibility to ethylene molecules. As a result, the sensor achieved a sensitivity of 51 Hz ppm<sup>-1</sup> with a detection limit of 420 ppb, demonstrating the effectiveness of the  $\text{Ag}^+$ -PVP composite in enhancing ethylene

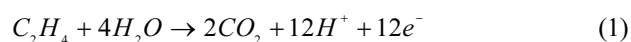
detection.

Despite its ability to detect ethylene at subppm levels, this sensor faces several limitations. Its narrow detection range (1–10 ppm) restricts its applicability in environments where ethylene concentrations frequently exceed 100 ppm. Additionally, selectivity remains a challenge, with response ratios for other VOCs ranging from 0.5 to 1.2, while the ethylene response ratio is only 3.9. Environmental factors such as fluctuations in temperature, humidity, and air pressure may induce frequency instability [53]. Moreover, continuous vibrations can lead to delamination of the sensing layer, increasing maintenance requirements. Addressing these limitations is essential for the practical implementation of QCM sensors in ethylene monitoring applications.

#### Electrochemical Sensors

Electrochemical sensors consist of a working electrode where ethylene undergoes oxidation, a counter electrode for the corresponding reduction reaction, and an electrolyte that enables ion transport. Ethylene detection is based on current changes induced by oxidation-reduction reactions at the electrode surfaces [54-56]:

Oxidation (at the working electrode):



Reduction (at the counter electrode):



Enhancements in sensor performance have been achieved through gas diffusion optimization, catalytic electrode modification, and membrane improvements. Toldra-Reig *et al.* [57] improved ethylene sensing by functionalizing  $\text{Fe}_{0.7}\text{Cr}_{1.3}\text{O}_3/8\text{YSZ}$  (yttria-stabilized zirconia) working electrodes with Ni

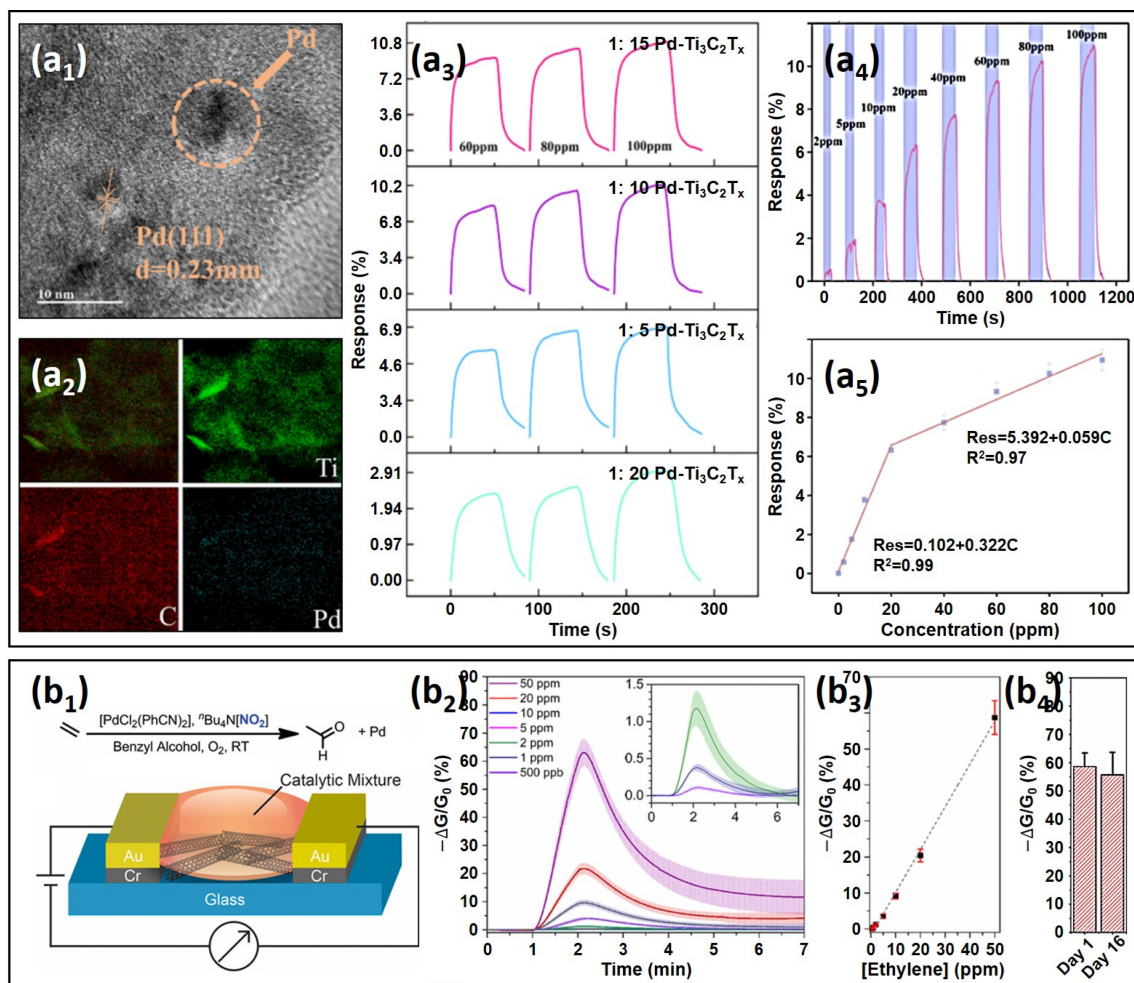


**Fig. 2.** MXene and CNT-based chemiresistive ethylene sensors: (a) Pd/Ti<sub>3</sub>C<sub>2</sub>T<sub>x</sub> MXene sensor: (a<sub>1</sub>) Transmission electron microscopy (TEM) image of Pd/Ti<sub>3</sub>C<sub>2</sub>T<sub>x</sub>. (a<sub>2</sub>) Elemental mapping of Pd/Ti<sub>3</sub>C<sub>2</sub>T<sub>x</sub>. (a<sub>3</sub>) Comparison of ethylene responses for different Pd functionalization contents. (a<sub>4</sub>) Sensor responses at varying ethylene concentrations. (a<sub>5</sub>) Calibration curve fitting ethylene concentration to sensor response. Reproduced with permission [82]. Copyright 2024, ACS. (b) Pd/Nitrite-4-Pyridyl SWCNT sensor: (b<sub>1</sub>) Schematic of the sensing device featuring Au electrodes on a glass substrate with an SWCNT network and liquid selector mixture. (b<sub>2</sub>) Ethylene sensitivity upon 1-minute exposure to ethylene in air. (b<sub>3</sub>) Calibration curve fitting ethylene concentration to sensor response. (b<sub>4</sub>) Sensor response before and after 16 days of storage at 4°C. Reproduced with permission [88]. Copyright 2020, ACS.

nanoparticles (NPs) (Fig. 1 (b)). The Ni NPs selectively catalyzed ethylene oxidation while suppressing CO oxidation, significantly enhancing the ethylene response and minimizing interference from competing gases such as CO. Electrochemical impedance spectroscopy confirmed that the Ni NPs improved the electrochemical oxidation of ethylene, leading to a stronger sensor signal.

Further improvements were achieved by replacing the conventional Pt reference electrode with lanthanum strontium manganite (LSM)/8YSZ. This strategy offered a cost-effective alternative while maintaining high ionic and catalytic activity for oxygen reduction, further stabilizing sensor operation.

Roy *et al.* [58] focused on membrane improvements, particularly in polyvinyl alcohol (PVA)-chitosan (CHT) membranes, which provide structural stability. The study

investigated graphene oxide (GO) functionalization within the PVA-CHT membrane, which significantly enhanced ethylene adsorption. The nanocrystalline multilayer structure of GO provided an extended electroactive surface area, increasing gas interaction and improving sensor sensitivity. In addition, the high electrical conductivity of GO facilitated efficient charge transfer, further enhancing ethylene sensing performance. As a result, the sensor achieved detection of 20 ppm ethylene while maintaining high selectivity by minimizing interference from competing gases such as ammonia, ethanol, and acetone.

Despite their high selectivity, electrochemical sensors still face challenges such as cross-sensitivity to acetylene, NO, and SO<sub>2</sub>, which can interfere with ethylene detection. Additionally, prolonged exposure to high ethylene concentrations can degrade the electrolyte, reducing the sensor lifespan [71].

Structural complexity, size constraints, and high manufacturing costs further limit large-scale deployment. Future research should focus on improving sensor stability, miniaturization, and cost-effectiveness to enable broader adoption in ethylene monitoring applications.

Although NDIR, QCM, and electrochemical sensors each offer distinct advantages, they are limited by their selectivity, stability, cost, and detection range (Table 2). The high production and maintenance costs of these sensors further restrict their widespread adoption in fresh produce distribution networks. Consequently, developing cost-effective and scalable sensors remains a critical research priority.

In this regard, chemiresistive sensors have emerged as promising alternatives, offering low-cost fabrication, simplified operation, and high scalability. The latest advancements in chemiresistive sensors for ethylene detection are discussed in the following section.

### 2.2.2 Chemiresistive Sensors: Strategies for Enhanced Response

The working principle of chemiresistive sensors is based on measuring changes in electrical resistance resulting from interactions between the sensing material and target gases [72]. Owing to their simple sensing mechanism, these sensors offer structural simplicity, cost-effectiveness, and easy integration into portable devices, making them ideal for use as widely accessible ethylene sensors. The primary sensing materials include MXenes, transition metal dichalcogenides (TMDs), carbon nanotubes (CNTs), reduced graphene oxide (rGO), and metal oxide semiconductors (MOS).

Chemiresistive sensors utilizing MXenes, TMDs, CNTs, and rGO generally operate at low or room temperature (RT), offering advantages such as cost reduction, energy efficiency, and safer operation [73–79]. However, because of ethylene's neutral molecular structure and low reactivity [80], sensors based on the pristine forms of these materials struggle to achieve high ethylene response (resistance ratio) and low detection limits at such low temperatures. Therefore, research efforts have primarily focused on enhancing ethylene response through catalyst decoration and composite material development.

#### *Electrophilic Catalyst Decoration*

The negligible ethylene response of pristine MXenes has been previously reported [81]. Guo *et al.* [82] proposed Pd<sup>2+</sup> surface functionalization as a strategy to enhance the ethylene sensing performance of Ti<sub>3</sub>C<sub>2</sub>T<sub>x</sub> MXene-based sensors (Fig. 2 (a)). The synthesis of the MXene involved LiF/HCl delamination of 200-mesh Ti<sub>3</sub>C<sub>2</sub>T<sub>x</sub> powders, followed by Pd<sup>2+</sup> functionalization through mixing with PdCl<sub>2</sub> solution.

The ethylene-sensing performance of the sensor was dependent on the amount of Pd. Specifically, sensors with Pd/

Ti<sub>3</sub>C<sub>2</sub>T<sub>x</sub> volume ratios of 1:5, 1:10, 1:15, and 1:20 exhibited responses of 6.9%, 10.2%, 10.9%, and 2.9%, respectively, when exposed to 100 ppm ethylene at 25°C. Notably, the sensor with a Pd/Ti<sub>3</sub>C<sub>2</sub>T<sub>x</sub> volume ratio of 1:15 demonstrated the highest ethylene response, enabling a linear response range from 2–20 ppm ethylene. These results demonstrate the critical role of Pd<sup>2+</sup> functionalization in enhancing the ethylene detection capabilities of MXene-based sensors.

The enhancement of ethylene sensing with Pd<sup>2+</sup> mainly arises from its strong interaction with ethylene's π bond. Ethylene has a carbon-carbon double bond, comprising a σ bond (formed by sp<sup>2</sup> hybrid orbitals) and a π bond (from the overlap of unhybridized p orbitals) [83]. Because π bond electrons are loosely held, they create an electron-rich region, making ethylene highly reactive toward electrophilic materials. Pd<sup>2+</sup>, with its [Kr]4d<sup>8</sup> configuration and two unpaired electrons [84], readily interacts with ethylene's electron-rich π bond, forming π-adsorbed ethylene species on the sensor surface. This interaction significantly alters the conductivity of Pd-MXenes, leading to pronounced chemiresistive variations upon ethylene exposure, making Pd<sup>2+</sup> an effective catalytic material for ethylene detection at RT.

The use of electrophilic catalysts for ethylene sensing has also been explored with TMD materials, such as MoS<sub>2</sub> [85]. Pramanik *et al.* [86] synthesized hydrothermally prepared MoS<sub>2</sub> and investigated the effects of electrophilic catalyst doping (0.34% Ni, 0.36% Fe, and 0.44% Co) on its sensing performance. Among the tested materials, Ni-doped MoS<sub>2</sub> (Ni-MoS<sub>2</sub>) exhibited the highest response of 21.2% upon exposure to 10 ppm ethylene at RT, whereas pristine MoS<sub>2</sub>, Co-MoS<sub>2</sub>, and Fe-MoS<sub>2</sub> showed lower responses of 0.2%, 1.5%, and 14.9%, respectively.

Density functional theory (DFT) calculations revealed that pristine MoS<sub>2</sub> had an adsorption energy of −0.186 eV, whereas Co-MoS<sub>2</sub>, Fe-MoS<sub>2</sub>, and Ni-MoS<sub>2</sub> exhibited values of −0.253, −0.257, and −0.673 eV, respectively. Charge transfer from the adsorbed ethylene to the sensing material followed the reverse order of the adsorption energy. Accordingly, the superior sensing performance of Ni-MoS<sub>2</sub> was attributed to the fact that it had the lowest ethylene adsorption energy and most efficient charge transfer to the sensing material.

These results suggest that electrophilic catalysts have the potential to enhance the ethylene response of MXene and TMD materials. However, electrophilicity is influenced not only by d-orbital configuration, but also by the oxidation state, charge density, and coordination geometry [87]. Additionally, charge transfer plays a crucial role in determining sensor performance. Therefore, the selection and application of electrophilic catalysts must be carefully optimized to maximize the ethylene response in such sensors.

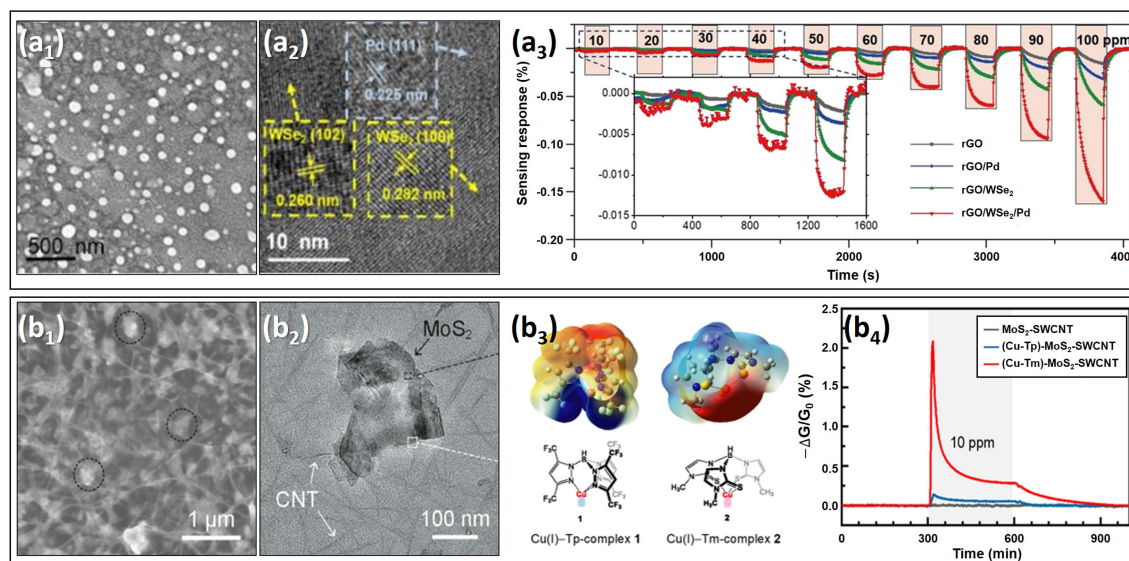


**Fig. 3.** Composite material-based chemiresistive ethylene sensors: (a) rGO/Pd/WSe<sub>2</sub> composite film sensor: (a<sub>1</sub>) SEM image of the rGO/Pd/WSe<sub>2</sub> composite film. (a<sub>2</sub>) TEM image of the rGO/Pd/WSe<sub>2</sub> composite film. (a<sub>3</sub>) Real-time sensing response of rGO-based self-assembled composite films to 10–100 ppm ethylene at RT. Reproduced with permission [90]. Copyright 2022, MDPI. (b) Cu<sup>+</sup>-pincer-MoS<sub>2</sub>-SWCNT composite sensor: (b<sub>1</sub>) SEM image of the MoS<sub>2</sub>-SWCNT composite. (b<sub>2</sub>) TEM image of the MoS<sub>2</sub>-SWCNT composite. (b<sub>3</sub>) Electrostatic potential maps of Cu-Tp and Cu-Tm, with red and blue surfaces indicating electron-rich and electron-deficient regions, respectively. (b<sub>4</sub>) Real-time response to 10 ppm ethylene for MoS<sub>2</sub>-SWCNT, (Cu-Tp)-MoS<sub>2</sub>-SWCNT, and (Cu-Tm)-MoS<sub>2</sub>-SWCNT sensors. Reproduced with permission [93]. Copyright 2020, ACS.

Fong *et al.* [88] proposed the surface functionalization of ligands alongside electrophilic catalyst-decorated materials as a strategy to further enhance the ethylene response (Fig. 2 (b)). They employed commercial single-walled CNTs (SWCNTs) as the sensing material and coated them with Bu<sub>4</sub>N[NO<sub>2</sub>] and PdCl<sub>2</sub>(PhCN)<sub>2</sub> via drop casting for surface functionalization of nitrate and Pd<sup>2+</sup>, respectively. The nitrate functionalization was applied to achieve the selective oxidation of ethylene [89].

Although the pristine SWCNT sensor exhibited almost no response to 50 ppm ethylene, the Pd/nitrate SWCNT sensor showed an improved response of 16%. Additional covalent functionalization of the sensor with 4-pyridyl via iodonium salt reactions further enhanced the ethylene response, reaching 58% when the degree of functionalization was up to 1.4 functional groups per 100 C atoms. This improvement was attributed to the regeneration of Pd<sup>2+</sup> from Pd<sup>0</sup> via the electron-donating role of 4-pyridyl ligands, which enhanced the charge transfer and stability of Pd<sup>2+</sup>. As a result, the sensor demonstrated a significantly low detection limit of 15 ppb and operated stably for more than 16 days. These results suggest that functionalizing electrophilic catalysts and ligands could be an effective strategy for enhancing the ethylene sensing performance of MXene-, TMD-, and CNT-based chemiresistive sensors. However, it is important to note that the non-covalent functionalization of 4-pyridyl via poly(vinyl pyridine) did not improve ethylene sensing performance. This indicates that the

functionalization methods and surface modification strategies should be carefully designed to ensure optimal ethylene response in these sensors.

#### Composite Material Development

Li *et al.* [90] reported enhanced ethylene sensing performance in rGO-based sensors by hybridizing rGO with Pd NPs and WSe<sub>2</sub> nanosheets (NSs) (Fig. 3 (a)). The sensor was fabricated by immersing a positively charged sensor substrate in a solution containing negatively charged rGO, Pd NPs, and WSe<sub>2</sub> NSs, followed by heat treatment.

The pristine rGO sensor showed a low response of 0.01% to 100 ppm ethylene at RT. However, the introduction of Pd NPs increased the response to 0.03%, likely due to the facilitated formation of  $\pi$ -adsorbed ethylene species, which enhanced electron transfer. The rGO/WSe<sub>2</sub> sensor further improved the ethylene response to 0.06%, which was attributed to the formation of rGO/WSe<sub>2</sub> heterojunctions [91].

When the rGO/WSe<sub>2</sub> heterojunctions were exposed to ethylene, the electron transfer from WSe<sub>2</sub> to the adsorbed ethylene molecules increased the hole concentration in WSe<sub>2</sub>. This increase in hole concentration led to a larger Fermi level difference between rGO and WSe<sub>2</sub>, which in turn facilitated greater hole transfer from WSe<sub>2</sub> to rGO [92]. Consequently, the chemiresistive variation of rGO upon ethylene exposure (ethylene response) increased.



Ultimately, the rGO/Pd/WSe<sub>2</sub> sensor exhibited the highest response of 0.16%, which was attributed to the synergistic effects arising from the combination of Pd and WSe<sub>2</sub>. These results suggest that modulating the charge distribution in the sensing material through composite development and harnessing the synergistic effects of chemical and electronic interactions are effective strategies for enhancing the response of rGO-based sensors.

Similarly, Chen *et al.* [93] developed highly sensitive ethylene sensors by hybridizing MoS<sub>2</sub>-SWCNT networks with Cu<sup>+</sup>-pincer complexes (Cu-Tm and Cu-Tb) (Fig. 3 (b)). The sensor was fabricated through the sequential drop-casting of MoS<sub>2</sub>-SWCNT followed by Cu-Tm or Cu-Tb functionalization and subsequent heat treatment.

While the pristine MoS<sub>2</sub>-SWCNT sensor exhibited a low response of ~0.7% to 10 ppm ethylene at RT, functionalization with Cu-Tm significantly enhanced the response to 2%. This improvement was primarily attributed to increased ethylene adsorption and charge transfer between Cu<sup>+</sup> and ethylene's  $\pi$ -bond, as well as the stabilization of Cu<sup>+</sup> by the electron-rich Tm ligand. In contrast, substituting the Tm ligand with the electron-withdrawing Tb ligand failed to enhance ethylene sensing, indicating that the electron-donating nature of Tm is essential for stabilizing Cu<sup>+</sup> and facilitating ethylene adsorption.

Once the surface catalysts facilitated ethylene adsorption and charge transfer, the heterojunction played a crucial role in amplifying the chemiresistive variation. As observed in the rGO/WSe<sub>2</sub> composite sensor, ethylene exposure increased the hole concentration in MoS<sub>2</sub>, thereby increasing the Fermi level difference between the SWCNT and MoS<sub>2</sub>. Thus, hole transfer to the SWCNT was promoted, enhancing the ethylene response. These results suggest that heterojunction formation through composite material design is an effective strategy for achieving high ethylene response in rGO-, MoS<sub>2</sub>-, and CNT-based chemiresistive sensors. However, efficient ethylene adsorption and charge transfer are essential prerequisites.

Although strategies such as electrophilic catalyst decoration and composite material development have demonstrated improved ethylene response in MXene-, TMD-, CNT-, and rGO-based sensors, their chemiresistive variation remains at percent levels, even when exposed to several tens of ppm of ethylene. Additionally, most of these sensors suffer from sluggish response and recovery times, often with poor reversibility, which pose challenges for monitoring trace ethylene levels in real-world environments.

Although MOS are considered a promising alternative, their ethylene-sensing performance at RT remains limited. For instance, Ag-ZnO has exhibited percent-level responses to tens of ppm ethylene and achieved a ppm-level detection limit [94], indicating that low-temperature operation is the primary lim-

itation affecting the low ethylene responses of MXene-, TMD-, CNT-, and rGO-based sensors.

MOS also exhibit suboptimal ethylene sensing performance at RT; however, unlike these materials, they have the advantage of operating at high temperatures. At elevated temperatures, MOS benefit from enhanced catalytic activity, enabling more sensitive and rapid ethylene detection. This suggests that MOS sensors operating at high temperatures hold significant potential for real-time monitoring of trace ethylene in fresh produce distribution networks. The following section discusses the underlying reactions responsible for highly sensitive ethylene sensing at elevated temperatures.

## 2.3 MOS-Based Ethylene Sensors: Sensing Mechanisms and Performance Enhancement Strategies

### 2.3.1 Sensing Mechanisms

MOS have been widely utilized in gas sensing applications owing to their simplicity, low cost, and ability to detect a wide range of gases with high response [3-6,95,96]. Their gas-sensing mechanisms are classified into n-type and p-type, depending on the primary charge carriers and the pathways through which these carriers conduct electricity (Fig. 4).

Under atmospheric conditions, oxygen molecules are adsorbed onto the MOS surface, withdrawing electrons and becoming ionized (O<sup>-</sup> at 200–400°C). This process forms either a resistive electron-depletion layer (EDL) in an n-type MOS, or a conductive hole-accumulation layer (HAL) in a p-type MOS. Consequently, a core-shell structure is formed, where n-type MOS materials exhibit a semiconducting core with a resistive shell, whereas p-type MOS materials have a semiconducting shell surrounding a resistive core.

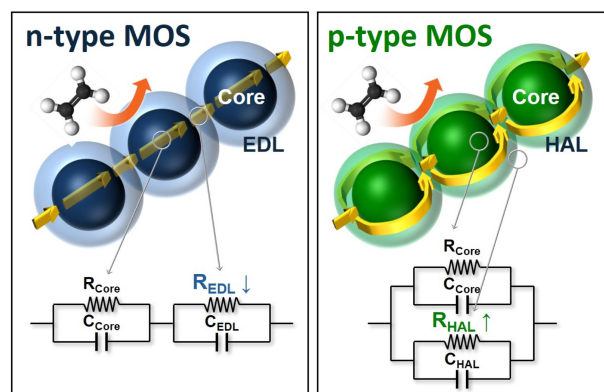


**Fig. 4.** Ethylene sensing mechanisms of n-type and p-type MOS: Upon exposure to ethylene, n-type MOS exhibit a decrease in resistance due to electron donation from ethylene oxidation, whereas p-type MOS exhibit an increase in resistance as hole concentration is reduced. These resistance changes enable ethylene detection.

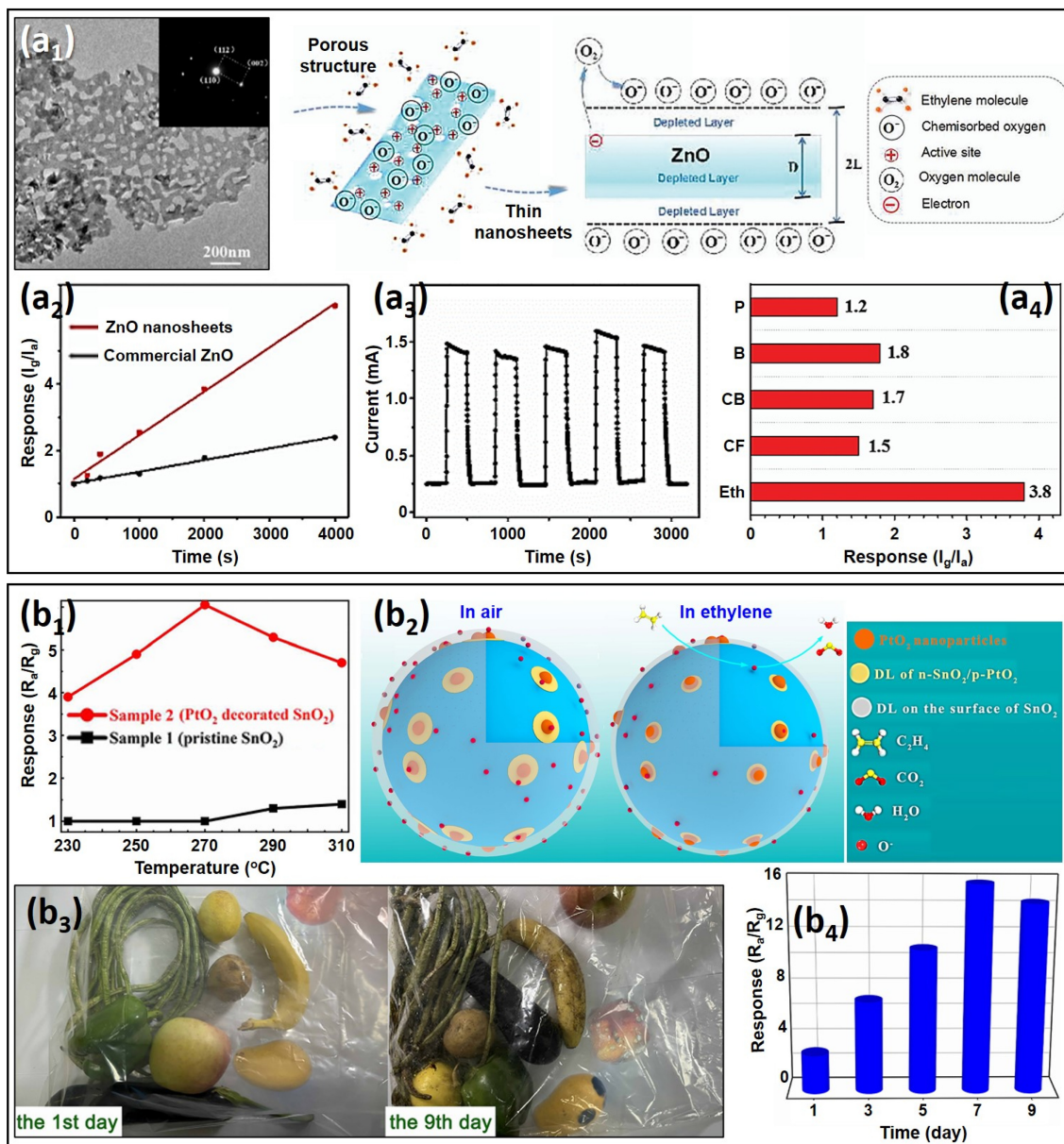


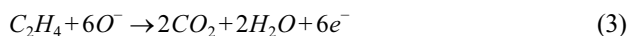
**Fig. 5.** ZnO and SnO<sub>2</sub>-based ethylene sensors: (a) ZnO NS sensor: (a<sub>1</sub>) TEM image of ZnO NSs. (a<sub>2</sub>) Comparison of ethylene responses between ZnO NSs and commercial ZnO sensors at 2000 ppm. (a<sub>3</sub>) Response curves of the ZnO NS sensor to 2000 ppm ethylene. (a<sub>4</sub>) Sensor responses to 500 ppm VOCs, including ethylene (Eth), chloroform (CF), chlorobenzene (CB), benzene (B), and phenixin (P). Reproduced with permission [101]. Copyright 2019, RSC. (b) PtO<sub>2</sub>-SnO<sub>2</sub> sensor: (b<sub>1</sub>) Ethylene responses of pristine SnO<sub>2</sub> and PtO<sub>2</sub>-SnO<sub>2</sub> sensors at 100 ppm. (b<sub>2</sub>) Schematic illustrating the origin of surface resistance variations in the sensor. (b<sub>3</sub>) Morphological changes of fruits and vegetables on the 1<sup>st</sup> and 9<sup>th</sup> test days. (b<sub>4</sub>) Sensor response to gases collected from 10 L bags containing aged fruits and vegetables. Reproduced with permission [103]. Copyright 2024, RSC.

In n-type MOS (*e.g.*, SnO<sub>2</sub>, ZnO, In<sub>2</sub>O<sub>3</sub>), the conductance is determined by the series connection between the semiconducting core and the resistive EDL. Even small changes in EDL thickness result in significant resistance shifts, enabling high chemiresistive variation. For example, reducing gases such as ethylene donate electrons through the following oxidation reaction, decreasing the EDL and leading to high chemiresistive variation.

In contrast, p-type MOS (*e.g.*, CuO, NiO, and Cr<sub>2</sub>O<sub>3</sub>) rely on parallel conduction pathways, where the interplay between the semiconducting shell and the resistive core determines the overall conductivity [97,98]. Owing to this structure, even substantial changes in HAL thickness result in only moderate resistance variations, making p-type MOS sensors generally less sensitive than n-type sensors [97,99].

However, p-type MOS materials can function as oxidation

catalysts because of their higher oxygen adsorption [97,100], allowing them to fully or partially oxidize ethylene through the following reactions:



Eq. (4) is particularly noteworthy because it converts ethylene into acetaldehyde, which is a more reactive species. This unique reforming reaction can be effectively utilized for enhanced ethylene sensing. Consequently, p-type MOS materials are also considered promising for achieving high ethylene response.

Overall, n-type MOS are particularly advantageous because of their high chemiresistive variation, whereas p-type MOS, although generally less sensitive, offer significant potential for enhanced ethylene response through ethylene reforming reactions. This demonstrates the potential of both MOS types in the development of highly sensitive ethylene sensors. However, to fully harness their capabilities, these sensors must operate at elevated temperatures, as key chemical reactions, such as those described in Eqs. (3) and (4), predominantly occur within this range. This fundamental principle highlights the suitability of high-temperature MOS sensors for highly sensitive ethylene detection.

### 2.3.2 High-Performance Ethylene Sensors: Strategies for Enhanced Response and Selectivity

Despite their potential, MOS sensors have also faced challenges regarding low response to ethylene because of its neutral molecular structure and low reactivity. Additionally, the gas selectivity (response ratio) remains a major challenge because MOS surfaces undergo indiscriminate oxidation/reduction reactions with various gases, leading to cross-sensitivity. To address these limitations, modern MOS sensors have adopted various strategies to enhance ethylene response and selectivity, including nanostructure design, noble metal catalyst decoration, composite material development, and bilayer film fabrication. Each of these approaches is explored in this section.

#### *Nanostructure Design*

Wang *et al.* [101] developed porous ZnO NSs and compared their ethylene sensing properties with those of commercial ZnO powders (Fig. 5 (a)). The porous ZnO NSs were synthesized using a wet-chemical method, followed by thermal annealing at 500°C. The commercial ZnO powders exhibited a response of ~2 (~200%) upon exposure to 2000 ppm ethylene at 500°C, already surpassing the performance of most RT sen-

sors. This confirmed the potential of high-temperature MOS sensors for highly sensitive ethylene sensing.

The porous ZnO NSs further improved the response to ~6 under the same conditions. In addition, the sensor exhibited rapid response (8 s) and recovery (20 s) times, along with high repeatability (tested over five cycles) and long-term stability for 30 days. This enhancement is attributed to their highly porous structure, which provides a large surface area for ethylene adsorption, and their single-crystalline nature, which minimizes grain boundary resistance and thereby facilitates efficient charge transfer. These results confirm the effectiveness of nanostructure design for achieving high ethylene response.

However, the ethylene response in this study was not sufficiently high, capable of tracing ppb-levels of ethylene. In addition, the selectivity value was as low as 2.11 against 500 ppm benzene, chlorobenzene, phenixin, and chloroform, limiting their practical applications. These limitations highlight the need for additional strategies to enhance surface reactions toward ethylene and improve ethylene response and selectivity.

#### *Noble Metal Catalyst Decoration*

Zhao *et al.* [102] designed an SnO<sub>2</sub> NP-based MOS sensor and decorated it with Pd NPs to enhance its ethylene response. The Pd NPs consisted of metallic Pd (Pd<sup>0</sup>, 42%) and PdO (Pd<sup>2+</sup>, 58%). Sensor measurements at 250°C showed that pure SnO<sub>2</sub> exhibited a response of 3.5 to 100 ppm ethylene, whereas Pd-SnO<sub>2</sub> achieved a threefold increase, reaching 11.1. This improvement was attributed to enhanced oxygen adsorption, facilitated by both the surface of the Pd NPs and the oxygen vacancies in SnO<sub>2</sub> generated by Pd doping, which promoted the oxidation of ethylene. Additionally, the formation of heterojunctions between Pd and SnO<sub>2</sub> contributed to maximizing chemiresistive variation upon ethylene exposure by extending the EDL.

The high response of the sensor enabled a low detection limit of 50 ppb, with high linearity ( $R^2 = 0.9963$ ) in the 0.05–1 ppm ethylene concentration range. Additionally, Pd NP decoration significantly reduced the response time from 7 s to 1 s, demonstrating its ability to accelerate ethylene detection. This confirms that Pd is an effective catalyst for enhancing the ethylene-sensing properties of MOS sensors, as it has been for RT sensors.

Li *et al.* [103] proposed the use of PtO<sub>2</sub> as a catalyst to enhance the ethylene sensing performance of SnO<sub>2</sub> NP-based sensors (Fig. 5 (b)). The PtO<sub>2</sub>-decorated SnO<sub>2</sub> NPs were synthesized using a sol-gel method, followed by annealing at 500°C.

The pristine SnO<sub>2</sub> NP sensor showed almost no response to 100 ppm ethylene at 270°C. However, after PtO<sub>2</sub> decoration, the ethylene response increased to ~6. Consequently, the sen-

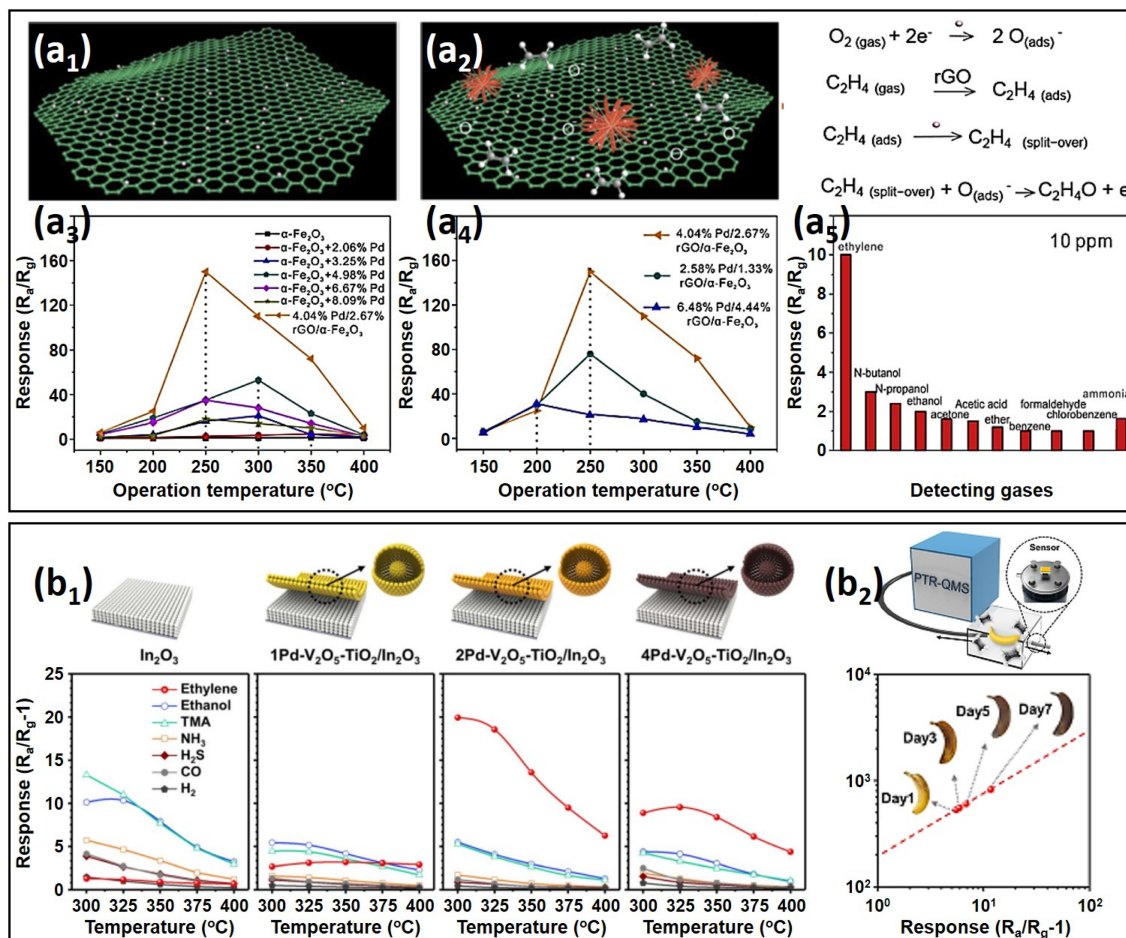


**Fig. 6.** Composite material design and bilayer film architecture used in ethylene sensors: (a) rGO/Pd/ $\alpha$ -Fe<sub>2</sub>O<sub>3</sub> composite sensor: (a<sub>1</sub>) Schematic illustration of the Pd/rGO composite structure. (a<sub>2</sub>) Schematic representation of the Pd/rGO/ $\alpha$ -Fe<sub>2</sub>O<sub>3</sub> composite. (a<sub>3</sub>) Ethylene responses of  $\alpha$ -Fe<sub>2</sub>O<sub>3</sub> and Pd/ $\alpha$ -Fe<sub>2</sub>O<sub>3</sub> composites with varying Pd contents at 1000 ppm. (a<sub>4</sub>) Ethylene responses of Pd/rGO/ $\alpha$ -Fe<sub>2</sub>O<sub>3</sub> composites with different Pd and rGO contents at 1000 ppm. (a<sub>5</sub>) Selectivity analysis of the 4.04% Pd/2.67% rGO/ $\alpha$ -Fe<sub>2</sub>O<sub>3</sub> composite sensor toward various VOCs at 250°C. Reproduced with permission [104]. Copyright 2019, Elsevier. (b) Pd-V<sub>2</sub>O<sub>5</sub>-TiO<sub>2</sub>/In<sub>2</sub>O<sub>3</sub> bilayer sensor: (b<sub>1</sub>) Responses of pristine In<sub>2</sub>O<sub>3</sub>, 1Pd-V<sub>2</sub>O<sub>5</sub>-TiO<sub>2</sub>/In<sub>2</sub>O<sub>3</sub>, 2Pd-V<sub>2</sub>O<sub>5</sub>-TiO<sub>2</sub>/In<sub>2</sub>O<sub>3</sub>, and 4Pd-V<sub>2</sub>O<sub>5</sub>-TiO<sub>2</sub>/In<sub>2</sub>O<sub>3</sub> sensors to 1 ppm of various gases across a temperature range of 300–400°C. (b<sub>2</sub>) Correlation between ethylene concentration during banana aging, measured by PTR-QMS ( $y$ -axis), and the gas response of the 2Pd-V<sub>2</sub>O<sub>5</sub>-TiO<sub>2</sub>/In<sub>2</sub>O<sub>3</sub> sensor ( $x$ -axis). Reproduced with permission [106]. Copyright 2023, RSC.

sensor achieved a low detection limit of 60 ppb with a linear response range ( $R^2 = 0.9816$ ) from 60 to 800 ppb, demonstrating its capability to detect trace levels of ethylene. The enhanced ethylene response was attributed to factors similar to those reported by Zhao *et al.*, including enhanced oxygen adsorption, oxygen vacancy formation, and heterojunction (p(PtO<sub>2</sub>)-n(SnO<sub>2</sub>)) junction) formation due to PtO<sub>2</sub> decoration.

In this study, the ethylene selectivity of the sensor was evaluated against 100 ppm ethanol, H<sub>2</sub>, NH<sub>3</sub>, NO, CO, putrescine, and cadaverine, with a selectivity value of  $\sim 2.5$ . Despite the limited ethylene selectivity, the sensor demonstrated real-time monitoring of ethylene emissions during the ripening and spoilage of various fruits and vegetables, including bananas, nectarines, mangoes, and apples. Although it was performed in a controlled environment, this study highlights the potential of

noble metal catalyst-decorated MOS sensors for real-time ethylene monitoring in fresh produce storage and distribution.

#### Composite Material Development

Li *et al.* [104] developed a composite sensor consisting of rGO, Pd NPs, and flower-like hierarchical porous  $\alpha$ -Fe<sub>2</sub>O<sub>3</sub>, demonstrating improved ethylene sensing properties (Fig. 6 (a)). The composite was synthesized using a wet-chemical method, where  $\alpha$ -Fe<sub>2</sub>O<sub>3</sub> was first prepared via a hydrothermal process. Subsequently, Pd NPs and rGO were self-assembled onto  $\alpha$ -Fe<sub>2</sub>O<sub>3</sub> under controlled stirring.

At an operating temperature of 250°C, the pure  $\alpha$ -Fe<sub>2</sub>O<sub>3</sub> sensor showed a low response of  $\sim 1.5$  to 1000 ppm ethylene. With the decoration of Pd NPs, the Pd/ $\alpha$ -Fe<sub>2</sub>O<sub>3</sub> sensor exhibited a significant increase in ethylene response, reaching  $\sim 40$  with

4.98% of Pd NPs, confirming the effectiveness of Pd catalysts in enhancing ethylene sensing performance.

Further improvements were observed upon the incorporation of rGO. The 2.67% rGO-hybridized sensor exhibited a notably enhanced ethylene response of  $\sim 150$  and enabled an ultra-low detection limit of 10 ppb. This remarkable improvement was attributed to rGO's unique physicochemical properties, which played a crucial role in optimizing sensor performance. First, the incorporation of rGO provided additional adsorption sites for ethylene, increasing the gas interaction probability at the sensor surface and enhancing the gas diffusion and adsorption efficiency. Moreover, rGO's high electrical conductivity facilitated charge transport, accelerating electron transfer within the composite and further amplifying the sensing response. These results highlight the potential of composite design for achieving higher ethylene responses. However, the sensor's selectivity toward 10 ppm ethylene against n-butanol, n-propanol, and ethanol was limited, indicating that achieving high ethylene selectivity remains a challenge.

#### Bilayer Film Fabrication

Although noble metal catalyst decoration and composite material development have significantly enhanced the response of MOS sensors, enabling the detection of ppb-level ethylene, ethylene selectivity remains the primary challenge in real-world applications. Another major limitation is the increase in sensor resistance caused by these modifications, which can hinder their integration into cost-effective portable devices.

To address these issues, MOS gas sensors with catalytic filtering layers have been introduced. These monolithic sensors feature a bilayer structure, where the MOS layer serves as the gas-sensing layer, and a catalytic filtering layer is deposited on top. This structural separation enables independent optimization of both sensing and filtering processes, mitigating challenges such as increased sensor resistance and indiscriminate enhancement of gas responses to both ethylene and non-target gases.

Although research on bilayer sensors for ethylene detection remains relatively limited, some studies have demonstrated their significant potential for improving ethylene selectivity. For instance, Jeong *et al.* [105] developed a bilayer ethylene sensor by applying a nanoscale  $\text{Cr}_2\text{O}_3$  overlayer to a  $\text{SnO}_2$  hollow sphere (HS) sensing layer. The  $\text{SnO}_2$  HSs and  $\text{Cr}_2\text{O}_3$  overlayer were prepared using ultrasonic spray pyrolysis and electron-beam evaporation, respectively.

Without the  $\text{Cr}_2\text{O}_3$  overlayer, the sensor exhibited indiscriminate responses to various gases. For example, the pristine  $\text{SnO}_2$  HS sensor displayed similar responses ( $\sim 12$ ) to both 2.5 ppm ethylene and trimethylamine (TMA) at  $375^\circ\text{C}$ , indicating a lack of ethylene selectivity. However, introducing a 50 nm-

thick  $\text{Cr}_2\text{O}_3$  overlayer significantly reduced the response to TMA while maintaining the ethylene response, thereby improving ethylene selectivity. Further increasing the  $\text{Cr}_2\text{O}_3$  overlayer thickness to 300 nm resulted in a higher ethylene selectivity of 4.9, with a minimal decrease in the ethylene response. However, when the overlayer thickness exceeded 300 nm, both the ethylene response and selectivity decreased. These results indicate the importance of optimizing the overlayer thickness to achieve optimal ethylene selectivity and response.

Similarly, Moon *et al.* [106] introduced a bilayer-structured ethylene sensor by applying a Pd- $\text{V}_2\text{O}_5$ - $\text{TiO}_2$  yolk-shell (YS) overlayer on an  $\text{In}_2\text{O}_3$  HS sensing layer (Fig. 6 (b)). The Pd- $\text{V}_2\text{O}_5$ - $\text{TiO}_2$  YSs and  $\text{In}_2\text{O}_3$  HSs were synthesized using ultrasonic spray pyrolysis, and the catalytic properties of the overlayer were adjusted by varying the Pd content (1–4 mol%) while keeping the other contents constant.

As observed in Jeong's study, the pristine  $\text{In}_2\text{O}_3$  HS sensor exhibited poor ethylene selectivity, with a low response of 1.2 to 1 ppm ethylene at  $325^\circ\text{C}$ . Notably, the response to ethanol, a representative reactive gas, was much higher ( $\sim 8$ ) than that to ethylene. Introducing a 1 mol% Pd- $\text{V}_2\text{O}_5$ - $\text{TiO}_2$  (1Pd- $\text{V}_2\text{O}_5$ - $\text{TiO}_2$ ) overlayer significantly reduced the responses to interfering gases, including ethanol, likely because of the strong oxidation properties of the Pd- $\text{V}_2\text{O}_5$ - $\text{TiO}_2$  catalyst toward VOC gases [107].

Interestingly, the ethylene response increased, becoming comparable to those of other gases. With a 2Pd- $\text{V}_2\text{O}_5$ - $\text{TiO}_2$  overlayer, the ethylene response increased significantly to 18.6, while the responses to other gases diminished, achieving a high ethylene selectivity of 4.7. This demonstrates that the catalytic overlayer not only oxidized interfering gases but also enhanced the ethylene response.

Considering that Pd- $\text{V}_2\text{O}_5$ - $\text{TiO}_2$  is a well-known catalyst for Wacker oxidation, it likely reforms ethylene into more reactive acetaldehyde, as described in Eq. (4). This suggests that the increase in the ethylene response can be attributed to the generation of reactive acetaldehyde, which undergoes further oxidation near the sensing electrodes. Consequently, even with a catalytic filtration layer, the ethylene response can remain high or even increase. This demonstrates that an appropriately designed filter layer does not always hinder the ethylene response, but can enhance both the response and selectivity.

These studies highlight the potential of bilayer film design for achieving both high ethylene response and selectivity. Notably, both approaches demonstrated real-time fruit ripeness monitoring by accurately tracking ethylene levels during fruit ripening, such as in bananas.

However, the complex gas composition in fresh produce distribution environments necessitates further validation of selec-

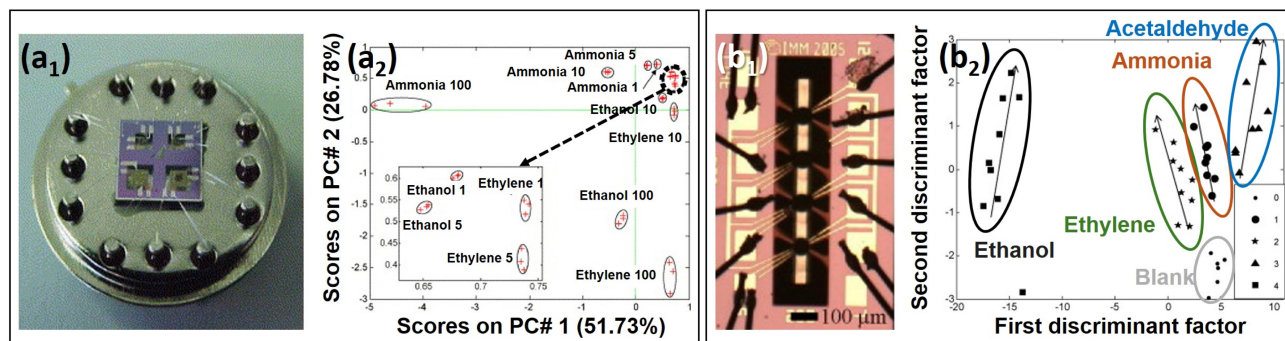


**Fig. 7.** MOS-based sensor arrays: (a)  $\text{SnO}_2$  and  $\text{WO}_3$ -based micro-hotplate sensor array: (a<sub>1</sub>) Optical image of a four-element micro-hotplate mounted on a standard support with an active sensing layer. (a<sub>2</sub>) PCA results performed on the responses of the four-element integrated microarray to individual gases, with auto-scaled data. Reproduced with permission [108]. Copyright 2005, Elsevier. (b) Four-element ULPH sensor array: (b<sub>1</sub>) Optical microscope image of a ULPH sensor array, with each element coated with a different gas-sensitive material using micro-drop coating. (b<sub>2</sub>) DFA results using responses from the four-element ULPH sensor array. (0) Blank measurements, (1) ammonia, (2) ethylene, (3) acetaldehyde, and (4) ethanol. Reproduced with permission [110]. Copyright 2010, Elsevier.

tive ethylene sensing for real-world applications. To enhance accuracy, integrating sensor arrays with advanced signal processing techniques may be essential. The next section explores sensor arrays for ethylene monitoring.

### 2.3.3 Sensor Arrays

Ivanov *et al.* [108] developed a micro-hotplate gas sensor array for ethylene monitoring, targeting key indicators of fruit ripeness and contamination in storage environments, such as ethylene, ethanol, and ammonia (Fig. 7 (a)). The sensor array comprised four MOS elements, utilizing  $\text{SnO}_2$  and  $\text{WO}_3$  as base materials with selective doping of Pt, Pd, and Au to enhance the response and selectivity.

Among these sensors, the  $\text{SnO}_2 + 1\% \text{ Pt}$  sensor exhibited the highest sensitivity to ethylene, making it the primary choice for ethylene detection. The  $\text{SnO}_2 + 1\% \text{ Pd}$  sensor showed the strongest response to ammonia, whereas the  $\text{SnO}_2 + 1\% \text{ Au}$  sensor demonstrated a high response to ethanol. The  $\text{WO}_3$  sensor included in the array was specifically designed to detect ammonia with a minimal cross-response to ethylene.

For signal analysis, the research team employed principal component analysis (PCA) for qualitative gas differentiation and a Fuzzy ARTMAP Neural Network for semi-quantitative classification [109]. PCA effectively separated the ethylene, ethanol, and ammonia responses, confirming the feasibility of distinguishing gases based on sensor data. The Fuzzy ARTMAP model further classified and quantified gas concentrations with a 100% success rate, demonstrating the system's capability for real-time ethylene monitoring.

Similarly, Espinosa *et al.* [110] developed an ultra-low-power hotplate (ULPH) gas sensor array for real-time ethylene detection (Fig. 7 (b)). This array consisted of four MOS elements, each doped with a different noble metal to enhance

selectivity and response. Among them, the  $\text{SnO}_2 + 1\% \text{ Pt}$  sensor exhibited the highest response to ethylene, making it the most suitable for ethylene detection. The  $\text{SnO}_2 + 1\% \text{ Pd}$  and  $\text{SnO}_2 + 1\% \text{ Au}$  sensors also responded to ethylene, but their cross-responses to ethanol and acetaldehyde, respectively, reduced their selectivity. The  $\text{WO}_3 + 1\% \text{ Pt}$  sensor showed a minimal ethylene response but demonstrated high sensitivity to ammonia.

Discriminant factor analysis (DFA) was applied to analyze the sensor array's response signals. This statistical model effectively distinguished ethylene from interfering gases such as ethanol, acetaldehyde, and ammonia. By minimizing intra-class variance, DFA ensured that ethylene responses remained tightly clustered, while maximizing inter-class variance allowed for better separation of different gas response patterns, enabling more accurate ethylene classification. As a result, DFA significantly improved ethylene discrimination accuracy and reduced false positives, enhancing the sensor array's ability to selectively detect ethylene.

The study demonstrated that the sensor array successfully differentiated ethylene from other gases, even at low concentrations (5–20 ppm), using DFA-based signal processing. With a low power consumption of 7 mW per microsensor at 350°C, the sensor array was well suited for battery-powered applications, making it viable for portable and handheld ethylene sensing devices. These results highlight the potential of MOS-based sensor arrays combined with machine learning techniques for real-time ethylene monitoring in fresh produce distribution networks.

### 2.3.4 Future Perspective and Opportunities

Although sensor arrays have demonstrated significant potential for ethylene detection in complex gas mixtures, their effec-

tiveness is limited when constructed using low-selectivity sensors. To investigate the impact of single-sensor selectivity on sensor array performance, Pineau *et al.* [111] compared two types of sensor arrays: an orthogonal sensor array consisting of ethanol (Si:SnO<sub>2</sub>), acetone (Si:WO<sub>3</sub>), and ammonia (Si:MoO<sub>3</sub>) sensors, and a collinear sensor array composed of three different SnO<sub>2</sub>-based ethanol sensors (Pd:SnO<sub>2</sub>, Pt:SnO<sub>2</sub>, Si:SnO<sub>2</sub>). These arrays were tested in 60 different gas mixtures containing ethanol, acetone, and ammonia, and their performance was evaluated by comparing the measured responses with the predicted values.

The orthogonal sensor array achieved high accuracy, with coefficients of determination ( $R^2$ ) close to 1, specifically 0.88 for ethanol, 0.99 for acetone, and 0.96 for ammonia. In contrast, the collinear sensor array exhibited significantly lower performance, with  $R^2$  values of 0.28 for ethanol, 0.86 for acetone, and 0.01 for ammonia. Notably, for ammonia, the collinear array performed even worse than a single Si:MoO<sub>3</sub> sensor, which had an  $R^2$  value of 0.68. This suggests that when an array is constructed with sensors that lack sufficient selectivity, the overall performance may degrade beyond that of an individual sensor. These findings emphasize the importance of selectivity in sensor array design, particularly for ethylene monitoring applications requiring precise differentiation from interfering gases.

Accordingly, future research should focus on enhancing the ethylene selectivity of individual sensors. Refining strategies such as catalyst decoration, nanostructure engineering, and bilayer sensor architectures can significantly improve sensor performance. Exploring novel MOS materials with intrinsic ethylene selectivity and alternative sensing mechanisms may further advance ethylene detection capabilities.

Ensuring consistent sensor performance is also crucial, considering the harsh and variable conditions of fresh produce distribution networks. Storage and transportation containers often experience high humidity and fluctuating oxygen and CO<sub>2</sub> concentrations, which are adjusted to regulate ripening. These environmental changes pose significant challenges for MOS sensors and arrays for real-world postharvest ethylene monitoring, necessitating sensor designs that can adapt to dynamic conditions while maintaining accuracy.

Another critical research direction is reducing the high operating temperatures of MOS sensors, which currently lead to increased energy consumption and sensor degradation over time. Developing low-power alternatives that maintain sensitivity at lower temperatures is essential for improving energy efficiency and extending sensor lifespan. The integration of AI-driven machine learning models into miniaturized sensor systems can further enhance classification accuracy, enabling precise ethylene detection even in complex gas environments.

The incorporation of MOS sensors into postharvest systems enables real-time ethylene monitoring throughout storage and transportation. This capability plays a pivotal role in ethylene management, allowing for the automated activation of ventilation systems and ethylene scrubbers to maintain optimal storage conditions. Additionally, temperature and humidity adjustments based on ethylene levels can help minimize over-ripening and prevent spoilage. Implementing dynamic storage segregation based on ethylene emission profiles can further reduce cross-contamination between ethylene-emitting and ethylene-sensitive produce, thereby extending shelf life and minimizing waste.

The integration of MOS sensors with Internet of Things (IoT) platforms presents exciting opportunities for automated and remote ethylene monitoring. By embedding MOS sensors into smart storage systems, agricultural stakeholders can gain greater control over postharvest processes, ensuring higher product quality and minimizing food losses. As MOS sensor technology evolves, the convergence of sensor arrays, AI-driven signal processing, and IoT-based monitoring will revolutionize ethylene sensing, making real-time, cost-effective, and highly selective ethylene detection a practical reality for fresh produce distribution networks.

### 3. CONCLUSIONS

Significant advancements have been made in ethylene sensor technologies, including optical, piezoelectric, electrochemical, and chemiresistive sensors. Among these, chemiresistive sensors have shown remarkable progress through electrophilic catalyst decoration and composite material development based on MXenes, TMDs, CNTs, and rGO. However, their limited ethylene response and frequently poor reversibility have led to the emergence of MOS sensors as a more viable solution. Recent advancements in MOS-based ethylene sensors have focused on enhancing their response and selectivity through nanostructure design, noble metal catalyst decoration, composite material development, and bilayer sensor architectures. These improvements have significantly enhanced ethylene detection capabilities, achieving ppb-level sensitivity and real-time monitoring. In addition, bilayer catalytic filtering layers have been demonstrated to improve ethylene selectivity by selectively oxidizing interfering gases while maintaining or amplifying the ethylene response. The integration of sensor arrays with advanced signal processing techniques, such as DFA and PCA, has further improved ethylene discrimination in complex gas environments, thereby presenting a powerful solution for postharvest ethylene management. Future research should prioritize the development of highly selective, reliable, and low-power MOS sensors, along with microscale sensor

arrays integrated with AI-driven machine learning models, to enable cost-effective and scalable ethylene monitoring solutions. Owing to their potential and versatility, MOS-based sensors are expected to remain central to advancements in ethylene detection.

### CRedit Authorship Contribution Statement

**Cheyeon Kim:** Conceptualization, Investigation, Writing - original draft. **Sang-Won Lee:** Investigation, Writing - original draft. Visualization. **Junha Hwang:** Investigation, Writing - original draft. Visualization. **Ji-Wook Yoon:** Supervision, Writing - review & editing, Funding acquisition.

### Declaration of Competing Interest

The authors declare that they have no known competing financial interests or personal relationships that could have appeared to influence the work reported in this paper.

### Acknowledgements

This work was carried out with the support of the “Cooperative Research Program for Agriculture Science and Technology Development (Project No. PJ016994),” Rural Development Administration, Republic of Korea.

## REFERENCES

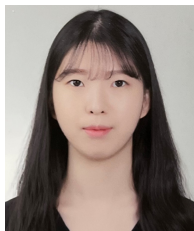
- [1] H. Yan, J. Wang, N. Shi, Y. Han, S. Zhang, G. Zhao, A flexible and wearable chemiresistive ethylene gas sensor modified with PdNPs-SWCNTs@Cu-MOF-74 nanocomposite: a targeted strategy for the dynamic monitoring of fruit freshness, *Chem. Eng. J.* 488 (2024) 151142.
- [2] X. Chen, R. Wreyford, N. Nasiri, Recent advances in ethylene gas detection, *Materials* 15 (2022) 5813.
- [3] J.-H. Lee, Gas sensors using hierarchical and hollow oxide nanostructures: Overview, *Sens. Actuators B Chem.* 140 (2009) 319–336.
- [4] N. Yamazoe, G. Sakai, K. Shimano, Oxide semiconductor gas sensors, *Catal. Surv. Asia* 7 (2003) 63–75.
- [5] K.J. Choi, H.W. Jang, One-dimensional oxide nanostructures as gas-sensing materials: Review and issues, *Sensors* 10 (2010) 4083–4099.
- [6] J. Zhang, X. Liu, G. Neri, N. Pinna, Nanostructured materials for room-temperature gas sensors, *Adv. Mater.* 28 (2016) 795–831.
- [7] B. Esser, J.M. Schnorr, T.M. Swager, Selective detection of ethylene gas using carbon nanotube-based devices: Utility in determination of fruit ripeness, *Angew. Chem. Int. Edit.* 51 (2012) 5752–5756.
- [8] A. Bleecker, Ethylene, *Curr. Biol.* 11 (2001) R952.
- [9] H. Lin, B.D. Freeman, Gas solubility, diffusivity and permeability in poly(ethylene oxide), *J. Membr. Sci.* 239 (2004) 105–117.
- [10] P.P. Power, Reactions of heavier main-group compounds with hydrogen, ammonia, ethylene and related small molecules, *Chem. Rec.* 12 (2012) 238–255.
- [11] A.D. Anggono, M. Rebezov, S. Mironov, L. Thangavelu, S. Aravindhan, A.M. Aljeboree, et al., Fruit preservation packaging technology based on air adjustment packaging method, *Food Sci. Technol.* 42 (2022) e29221.
- [12] A.A. Kader, *Postharvest Technology of Horticultural Crops*, third ed., ANR Publication, University of California, Oakland, 2002.
- [13] M.J. Serradilla, N. Falagán, B. Bohmer, L.A. Terry, M.C. Alamar, The role of ethylene and 1-MCP in early-season sweet cherry ‘Burlat’ storage life, *Sci. Hortic.* 258 (2019) 108787.
- [14] J.-H. Cai, S.-C. Cheng, F. Luo, Y.-B. Zhao, B.-D. Wei, Q. Zhou, et al., Influence of ethylene on morphology and pigment changes in harvested broccoli, *Food Bioprocess Technol.* 12 (2019) 883–895.
- [15] K. Papoutsis, Sustainable postharvest treatments for prolonging asparagus (*Asparagus officinalis* L.) shelf life by minimizing the development of physiological disorders, *ACS Food Sci. Technol.* 3 (2023) 1617–1631.
- [16] B.M. Hurr, D.J. Huber, C.E. Vallejos, S.T. Talcott, Developmentally dependent responses of detached cucumber (*Cucumis sativus* L.) fruit to exogenous ethylene, *Postharvest Biol. Technol.* 52 (2009) 207–215.
- [17] S. Gu, L. Xie, Q. Guan, X. Sheng, Y. Fang, X. Wang, Effect of ethylene production by four pathogenic fungi on the postharvest diseases of green pepper (*Capsicum annuum* L.), *Int. J. Food Microbiol.* 418 (2024) 110729.
- [18] M. Zhou, S. Guo, J. Zhang, H. Zhang, C. Li, X. Tang, et al., Comparative dynamics of ethylene production and expression of the ACS and ACO genes in normal-ripening and non-ripening watermelon fruits, *Acta Physiol. Plant.* 38 (2016) 228.
- [19] L.-Y. Chang, J.K. Brecht, Responses of 1-methylcyclopropene (1-MCP)-treated banana fruit to pre- and post-treatment ethylene exposure, *Sci. Hortic.* 309 (2023) 111636.
- [20] T. Zhu, W.-R. Tan, X.-G. Deng, T. Zheng, D.-W. Zhang, H.-H. Lin, Effects of brassinosteroids on quality attributes and ethylene synthesis in postharvest tomato fruit, *Postharvest Biol. Technol.* 100 (2015) 196–204.
- [21] T. Yan, C. Hu, Y. Que, Y. Song, D. Lu, J. Gu, et al., Chitosan coating enriched with biosynthetic CuO NPs: Effects on postharvest decay and quality of mango fruit, *Int. J. Biol. Macromol.* 253 (2023) 126668.
- [22] M. Knee, S.G.S. Hatfield, Benefits of ethylene removal during apple storage, *Ann. Appl. Biol.* 98 (1981) 157–165.
- [23] M.L. Arpaia, S. Collin, J. Sievert, D. Obenland, ‘Hass’ avocado quality as influenced by temperature and ethylene prior to and during final ripening, *Postharvest Biol. Technol.* 140 (2018) 76–84.
- [24] H.-Y. Xu, Y.-Y. Chen, L.-B. Wang, Z.-H. Xie, C. Gu, S.-L. Zhang, Transcriptome analysis reveals a regulation of ethylene-induced post-harvest senescence in pear fruit, *Sci. Hortic.* 240 (2018) 585–591.
- [25] E.K. Akamine, T. Goo, Respiration and ethylene production in mammee apple (*Mammea americana* L.), *J. Amer. Soc. Hort. Sci.* 103 (1978) 308–310.
- [26] A. Pongener, V. Sagar, R.K. Pal, R. Asrey, R.R. Sharma,



- S.K. Singh, Physiological and quality changes during post-harvest ripening of purple passion fruit (*Passiflora edulis* Sims), *Fruits* 69 (2014) 19–30.
- [27] G. Martinez, M. Serrano, M.T. Pretel, F. Riquelme, F. Romojaro, Ethylene biosynthesis and physico-chemical changes during fruit ripening of cherimoya (*Annona cherimola*, Mill), *J. Horticultural Sci.* 68 (1993) 477–483.
- [28] U. Nasir, A. Ismail, M. Riaz, K. Razzaq, S. Ali, A. Hussain, et al., Exploring fruit ripening methods: Conventional, artificial, and novel approaches for quality and health, *Food Control*. 165 (2024) 110626.
- [29] C.L. Girardi, A.R. Corrent, L. Lucchetta, M.R. Zanuzo, T.S. da Costa, A. Brackmann, et al., Effect of ethylene, intermittent warming and controlled atmosphere on postharvest quality and the occurrence of woolliness in peach (*Prunus persica* cv. Chiripá) during cold storage, *Postharvest Biol. Technol.* 38 (2005) 25–33.
- [30] R.B.H. Wills, V.V.V. Ku, D. Shohet, G.H. Kim, Importance of low ethylene levels to delay senescence of non-climacteric fruit and vegetables, *Aust. J. Exp. Agric.* 39 (1999) 221–224.
- [31] A. Kume, N. Tsuboi, N. Nakatani, K. Nakane, N. Sakurai, N. Nakagawa, et al., Measurement of ethylene emission from Japanese red pine (*Pinus densiflora*) under field conditions in NO<sub>x</sub>-polluted areas, *Environ. Pollut.* 111 (2001) 389–394.
- [32] H. Pham-Tuan, J. Vercammen, C. Devos, P. Sandra, Automated capillary gas chromatographic system to monitor ethylene emitted from biological materials, *J. Chromatogr. A* 868 (2000) 249–259.
- [33] S.M. Cristescu, E. Woltering, C. Hermans, F.J.M. Harren, S. te Lintel Hekkert, Research Tools: Ethylene Detection, In: C.-K. Wen (Eds.), *Ethylene in Plants*, Springer, Dordrecht, 2015, pp. 263–286.
- [34] C. Soukoulis, L. Cappellin, E. Aprea, F. Costa, R. Viola, T.D. Märk, et al., PTR-ToF-MS, a novel, rapid, high sensitivity and non-invasive tool to monitor volatile compound release during fruit post-harvest storage: the case study of apple ripening, *Food Bioprocess Technol.* 6 (2013) 2831–2843.
- [35] P. Sulzer, A. Edtbauer, E. Hartungen, S. Jürschik, A. Jordan, B. Hanel, et al., From conventional proton-transfer-reaction mass spectrometry (PTR-MS) to universal trace gas analysis, *Int. J. Mass Spectrom.* 321–322 (2012) 66–70.
- [36] L. Cappellin, S. Makhoul, E. Schuhfried, A. Romano, J. Sánchez del Pulgar, E. Aprea, et al., Ethylene: Absolute real-time high-sensitivity detection with PTR/SRI-MS. The example of fruits, leaves and bacteria, *Int. J. Mass Spectrom.* 365–366 (2014) 33–41.
- [37] G. Hübner, G. Rauhut, H. Stoll, E. Roduner, FTIR measurements and quantum chemical calculations of ethylene adsorbed on CuNaY, *Phys. Chem. Chem. Phys.* 4 (2002) 3112–3121.
- [38] F. Guo, R.-X. Li, S. Yang, X.-Y. Zhang, H. Yu, J.J. Urban, et al., Designing heteroatom-codoped iron metal–organic framework for promotional photoreduction of carbon dioxide to ethylene, *Angew. Chem.-Int. Edit.* 62 (2023) e202216232.
- [39] H.W.A. Berkelmans, B.W.M. Moeskops, J. Bominaar, P.T.J. Scheepers, F.J.M. Harren, Pharmacokinetics of ethylene in man by on-line laser photoacoustic detection, *Toxicol. Appl. Pharmacol.* 190 (2003) 206–213.
- [40] M. Giglio, A. Elefante, P. Patimisco, A. Sampaolo, F. Sgobba, H. Rossmadl, et al., Quartz-enhanced photoacoustic sensor for ethylene detection implementing optimized custom tuning fork-based spectrophone, *Opt. Express* 27 (2019) 4271–4280.
- [41] Z. Liao, J. Zhang, Z. Gan, Y. Wang, J. Zhao, T. Chen, et al., Thermal runaway warning of lithium-ion batteries based on photoacoustic spectroscopy gas sensing technology, *Int. J. Energy Res.* 46 (2022) 21694–21702.
- [42] G. Magnotti, U. KC, P.L. Varghese, R.S. Barlow, Raman spectra of methane, ethylene, ethane, dimethyl ether, formaldehyde and propane for combustion applications, *J. Quant. Spectrosc. Radiat. Transf.* 163 (2015) 80–101.
- [43] M.F. Mrozek, M.J. Weaver, Periodic trends in electrode-chemisorbate bonding: Ethylene on platinum-group and gold electrodes as probed by surface-enhanced Raman spectroscopy, *J. Phys. Chem. B* 105 (2001) 8931–8937.
- [44] Y. Yang, H. Bian, Z. Jia, P. Tu, Design and preparation of ethylene fluorescence probes based on arylolefins and Grubbs catalysts, *ACS Omega* 8 (2023) 15350–15359.
- [45] Y.-P. Lee, G.C. Pimentel, Chemiluminescence of ethylene in an inert matrix and the probable infrared spectrum of methylene, *J. Chem. Phys.* 75 (1981) 4241.
- [46] R.K. Jha, Non-dispersive infrared gas sensing technology: A review, *IEEE Sens. J.* 22 (2022) 6.
- [47] J. Kathirvelan, R. Vijayaraghavan, An infrared based sensor system for the detection of ethylene for the discrimination of fruit ripening, *Infrared Phys. Technol.* 85 (2017) 403–409.
- [48] Y. Zhang, P. Jiang, W. Cao, X. Li, J. Lai, High-sensitivity ethylene gas sensor based on NDIR and dual-channel lock-in amplifier, *Optik* 223 (2020) 165630.
- [49] J. Yun, M. Cho, K. Lee, M. Kang, I. Park, A review of nanostructure-based gas sensors in a power consumption perspective, *Sens. Actuators B Chem.* 372 (2022) 132612.
- [50] M. Wang, J. Huang, Q.-A. Huang, Putting piezoelectric sensors into Fano resonances, *Microsyst. Nanoeng.* 10 (2024) 202.
- [51] L. Rodríguez-Pardo, J. Fariña Rodríguez, C. Gabrielli, H. Perrot, R. Brendel, Sensitivity, noise, and resolution in QCM sensors in liquid media, *IEEE Sens. J.* 5 (2005) 1251–1257.
- [52] M.A.K.P. Tolentino, D.R.B. Albano, F.B. Sevilla III, Piezoelectric sensor for ethylene based on silver(I)/polymer composite, *Sens. Actuators B Chem.* 254 (2018) 299–306.
- [53] X. Ding, J. Li, K. Tang, X. Chen, H. Li, A highly linear and sensitive QCM humidity sensor based on high-frequency quartz crystal transducer, *IEEE Trans. Instrum. Meas.* 73 (2024) 9504009.
- [54] A.B. Olabintan, A.S. Abdullahi, B.O. Yusuf, S.A. Ganiyu, T.A. Saleh, C. Basheer, Prospects of polymer Nanocomposite-Based electrochemical sensors as analytical devices for environmental Monitoring: A review, *Microchem. J.* 204 (2024) 111053.

- [55] M.-Y. Kim, K. H. Lee, Electrochemical sensors for sustainable precision agriculture—A review, *Front. Chem.* 10 (2022) 848320.
- [56] L. Ma, L. Wang, R. Chen, K. Chang, S. Wang, X. Hu, et al., A low cost compact measurement system constructed using a smart electrochemical sensor for the real-time discrimination of fruit ripening, *Sensors* 16 (2016) 501.
- [57] F. Toldra-Reig, J.M. Serra, Surface functionalization with Ni of  $\text{Fe}_{0.7}\text{Cr}_{1.3}\text{O}_3/8\text{YSZ}$  electrode in a potentiometric sensor to selectively detect  $\text{C}_2\text{H}_4$ , *ACS Appl. Nano Mater.* 1 (2018) 6666–6673.
- [58] D. Roy, S. Gandhi, R. Gal-Oz, S. Vernick, M. Ghosh, A novel electroactive biopolymer-graphene oxide nanocomposite membrane for high-performance electrochemical sensing of ethylene, *Appl. Mater. Today* 39 (2024) 102291.
- [59] A. Sklorz, S. Janßen, W. Lang, Detection limit improvement for NDIR ethylene gas detectors using passive approaches, *Sens. Actuators B Chem.* 175 (2012) 246–254.
- [60] A. Eberhardt, K. Schmitt, J. Wöllenstein, Rotating interference filter spectrometer for the detection of ethylene in the ripening process of climacteric fruit, *Proceedings of the 2017 19th International Conference on Solid-State Sensors, Actuators and Microsystems (TRANSDUCERS)*, Kaohsiung, Taiwan, 2017, pp. 1445–1448.
- [61] J. Fonollosa, B. Halford, L. Fonseca, J. Santander, S. Udina, M. Moreno, et al., Ethylene optical spectrometer for apple ripening monitoring in controlled atmosphere store-houses, *Sens. Actuators B Chem.* 136 (2009) 546–554.
- [62] J. Hildenbrand, J. Wöllenstein, S. Hartwig, A. Eberhardt, B. Halford, M. Moreno, et al., A compact optical multichannel system for ethylene monitoring, *Microsyst. Technol.* 14 (2008) 637–644.
- [63] M. De Biasio, R. Leitner, C. Krall, M. Krivec, A. Wilk, B. Mizaikoff, et al., Ethylene gas sensing using non-dispersive infrared spectroscopy, *Proceedings of the 2016 IEEE Sensors, Orlando, USA, 2016*, pp. 1–3.
- [64] P. Sun, H. Han, X.-C. Xia, J.-Y. Dai, K.-Q. Xu, W.-H. Zhang, et al., Towards an E-nose: metal-organic frameworks based quartz crystal microbalance array for fruit ripeness indexing, *Talanta* 269 (2024) 125484.
- [65] B. Graewe, A. Rang, C.A. Schalley, J. Haubrich, J. Bargon, First gravimetric detection of ethene utilizing metallo-supramolecular macrocycles as sensor-active substances, *Sens. Actuators B Chem.* 119 (2006) 302–307.
- [66] L.R. Jordan, P.C. Hauser, G.A. Dawson, Amperometric sensor for monitoring ethylene, *Anal. Chem.* 69 (1997) 558–562.
- [67] R. Shekarriz, A high sensitivity continuous ethylene monitoring device for postharvest applications, *Proc. Fla. State Hort. Soc.* 120 (2007) 251–255.
- [68] F. Toldra-Reig, D. Pastor, J.M. Serra, Influence of the solid-electrolyte ionic material in a potentiometric sensor for ethylene detection, *J. Electrochem. Soc.* 166 (2019) B1343–B1355.
- [69] R. Shekarriz, W.L. Allen, Nanoporous gold electrocatalysis for ethylene monitoring and control, *Eur. J. Hortic. Sci.* 73 (2008) 171–176.
- [70] A. Huč, R. Vidrih, M. Trebar, Determination of pears ripening stages based on electrochemical ethylene sensor, *IEEE Sens. J.* 20 (2020) 13976–13983.
- [71] H. Wan, Y. Gan, J. Sun, T. Liang, S. Zhou, P. Wang, High sensitive reduced graphene oxide-based room temperature ionic liquid electrochemical gas sensor with carbon-gold nanocomposites amplification, *Sens. Actuators B Chem.* 299 (2019) 126952.
- [72] P. Najafi, A. Ghaemi, Chemiresistor gas sensors: Design, challenges, and strategies: A comprehensive review, *Chem. Eng. J.* 498 (2024) 154999.
- [73] D.H. Shin, Y.S. Choi, S.Y. Park, C.-S. Yeo, Y.Y. Park, J.Y. Song, et al., Fast and complete recovery of TMDs-decorated rGO fiber gas sensors at room temperature, *Appl. Surf. Sci.* 578 (2022) 151832.
- [74] D. Li, H. Liang, Y. Zhang, MXene-based gas sensors: State of the art and prospects, *Carbon* 226 (2024) 119205.
- [75] A. Mirzaei, J.-Y. Kim, H.W. Kim, S.S. Kim, Resistive Gas Sensors Based on 2D TMDs and MXenes, *Accounts Chem. Res.* 57 (2024) 2395–2413.
- [76] A. Kumar, A. Mirzaei, M.H. Lee, Z. Ghahremani, T.-U. Kim, J.-Y. Kim, et al., Strategic review of gas sensing enhancement ways of 2D tungsten disulfide/selenide-based chemiresistive sensors: decoration and composite, *J. Mater. Chem. A* 12 (2024) 3771–3806.
- [77] I. Raya, H.H. Kzar, Z.H. Mahmoud, A.A. Ahmed, A.Z. Ibatova, E. Kianfar, A review of gas sensors based on carbon nanomaterial, *Carbon Lett.* 32 (2022) 339–364.
- [78] R. Ghosh, M. Aslam, H. Kalita, Graphene derivatives for chemiresistive gas sensors: A review, *Mater. Today Commun.* 30 (2022) 103182.
- [79] F. Yi, H. Ren, J. Shan, X. Sun, D. Wei, Z. Liu, Wearable energy sources based on 2D materials, *Chem. Soc. Rev.* 47 (2018) 3152–3188.
- [80] B. Esser, J.M. Schnorr, T.M. Swager, Selective detection of ethylene gas using carbon nanotube-based devices: Utility in determination of fruit ripeness, *Angew. Chem. Int. Edit.* 51 (2012) 5752–5756.
- [81] X. Li, R. Sun, J. Pan, Z. Shi, J. Lv, Z. An, et al., All-MXene-printed RF resonators as wireless plant wearable sensors for in situ ethylene detection, *Small* 19 (2023) 2207889.
- [82] L. Guo, S. Chu, Y. Li, W. Huang, X. Wang, Flexible wearable chemoresistive ethylene gas-monitoring device utilizing  $\text{Pd/Ti}_3\text{C}_2\text{T}_x$  nanocomposites for in situ nondestructive monitoring of kiwifruit ripeness, *ACS Appl. Mater. Interfaces* 16 (2024) 49508–49519.
- [83] C.Y. Ma, Z. Mu, J.J. Li, Y.G. Jin, J. Cheng, G.Q. Lu, et al., Mesoporous  $\text{Co}_3\text{O}_4$  and  $\text{Au/Co}_3\text{O}_4$  catalysts for low-temperature oxidation of trace ethylene, *J. Am. Chem. Soc.* 132 (2010) 2608–2613.
- [84] L.M. Mirica, J.R. Khusnutdinova, Structure and electronic properties of Pd(III) complexes, *Coord. Chem. Rev.* 257 (2013) 299–314.
- [85] A. Wang, L. Zhang, Z. Yu, S. Zhang, L. Li, Y. Ren, et al., Ethylene methoxycarbonylation over heterogeneous  $\text{Pt}_1/\text{MoS}_2$  single-atom catalyst: Metal-support concerted catalysis, *J. Am. Chem. Soc.* 146 (2024) 695–706.
- [86] M. Pramanik, B. Jana, A. Ghatak, K. Das, Improvement in

- efficiency of MoS<sub>2</sub> nanoflower based ethylene gas sensor on transition metal doping: An experimental and theoretical investigation, *Mater. Chem. Phys.* 314 (2024) 128892.
- [87] A. Mirzaei, J.H. Bang, S.S. Kim, H.W. Kim, Effect of noble metals on hydrogen sensing properties of metal oxide-based gas sensors, *J. Sens. Sci. Technol.* 29 (2020) 365–368.
- [88] D. Fong, S.-X. L. Luo, R. S. Andre, T.M. Swager, Trace ethylene sensing via Wacker oxidation, *ACS Cent. Sci.* 6 (2020) 507–512.
- [89] Z.K. Wickens, B. Morandi, R.H. Grubbs, Aldehyde-selective Wacker-type oxidation of unbiased alkenes enabled by a nitrite co-catalyst, *Angew. Chem. Int. Edit.* 52 (2013) 11257–11260.
- [90] X. Li, C. Xu, X. Du, Z. Wang, W. Huang, J. Sun, et al., Assembled reduced graphene oxide/tungsten diselenide/Pd heterojunction with matching energy bands for quick banana ripeness detection, *Foods* 11 (2022) 1879.
- [91] A. Hussain, M.N. Lakhan, I.A. Soomro, M. Ahmed, A. Hanan, A.A. Maitlo, et al., Preparation of reduced graphene oxide decorated two-dimensional WSe<sub>2</sub> nanosheet sensor for efficient detection of ethanol gas, *Physica E* 147 (2023) 115574.
- [92] Y. Zu, C. He, D. Liu, L. Chen, W. Li, W. Zhang, Nonlinear optical properties of poly (vinyl alcohol) thin films doped with in-situ WSe<sub>2</sub>/rGO composite, *Opt. Laser Technol.* 142 (2021) 107198.
- [93] W.Y. Chen, A. Yermembetova, B.M. Washer, X. Jiang, S.N. Shuvo, D. Peroulis, et al., Selective detection of ethylene by MoS<sub>2</sub>-carbon nanotube networks coated with Cu(I)-pincer complexes, *ACS Sens.* 5 (2020) 1699–1706.
- [94] R. Jaisutti, S. Khemphet, S. Pudwat, N. Petchsang, Y.-H. Kim, T. Osotchan, et al., UV-induced room-temperature ethylene sensors based on Ag-decorated ZnO nanoflowers for fruit ripeness monitoring, *ACS Appl. Nano Mater.* 7 (2024) 16575–16584.
- [95] J.-W. Yoon, J.-H. Lee, Toward breath analysis on a chip for disease diagnosis using semiconductor-based chemiresistors: recent progress and future perspectives, *Lab Chip* 17 (2017) 3537–3557.
- [96] J.-W. Yoon, J.-H. Lee, Recent developments in metal oxide gas sensors for breath analysis, *Ceramist* 22 (2019) 70–81.
- [97] H.-J. Kim, J.-H. Lee, Highly sensitive and selective gas sensors using p-type oxide semiconductors: Overview, *Sens. Actuators B Chem.* 192 (2014) 607–627.
- [98] J.-W. Yoon, H.-J. Kim, H.-M. Jeong, J.-H. Lee, Gas sensing characteristics of p-type Cr<sub>2</sub>O<sub>3</sub> and Co<sub>3</sub>O<sub>4</sub> nanofibers depending on inter-particle connectivity, *Sens. Actuators B Chem.* 202 (2014) 263–271.
- [99] S. Pokhrel, C.E. Simion, V. Quemener, N. Bârsan, U. Weimar, Investigations of conduction mechanism in Cr<sub>2</sub>O<sub>3</sub> gas sensing thick films by ac impedance spectroscopy and work function changes measurements, *Sens. Actuators B Chem.* 133 (2008) 78–83.
- [100] M. Iwamoto, Y. Yoda, N. Yamazoe, T. Seiyama, Study of metal oxide catalysts by temperature programmed desorption. 4. Oxygen adsorption on various metal oxides, *J. Phys. Chem.* 82 (1978) 2564–2570.
- [101] L.-P. Wang, Z. Jin, T. Luo, Y. Ding, J.-H. Liu, X.-F. Wang, et al., The detection of ethylene using porous ZnO nanosheets: utility in the determination of fruit ripeness, *New J. Chem.* 43 (2019) 3619–3624.
- [102] Q. Zhao, Z. Duan, Z. Yuan, X. Li, S. Wang, B. Liu, et al., High performance ethylene sensor based on palladium-loaded tin oxide: Application in fruit quality detection, *Chin. Chem. Lett.* 31 (2020) 2045–2049.
- [103] C. Li, X. You, X. Zhao, P. Yin, X. Liu, F. Song, et al., A highly sensitive ethylene gas sensor based on PtO<sub>2</sub>-decorated SnO<sub>2</sub> used to monitor the ripening and spoilage of fruits and vegetables that are stored at room temperature, *New J. Chem.* 48 (2024) 10686–10696.
- [104] B. Li, M. Li, F. Meng, J. Liu, Highly sensitive ethylene sensors using Pd nanoparticles and rGO modified flower-like hierarchical porous  $\alpha$ -Fe<sub>2</sub>O<sub>3</sub>, *Sens. Actuators B Chem.* 290 (2019) 396–405.
- [105] S.-Y. Jeong, Y.K. Moon, T.-H. Kim, S.-W. Park, K.B. Kim, Y.C. Kang, et al., A new strategy for detecting plant hormone ethylene using oxide semiconductor chemiresistors: Exceptional gas selectivity and response tailored by nanoscale Cr<sub>2</sub>O<sub>3</sub> catalytic overlayer, *Adv. Sci.* 7 (2020) 1903093.
- [106] Y.K. Moon, J.H. Kim, S.-Y. Jeong, S.M. Lee, S.J. Park, T.H. Kim, et al., Exclusive detection of ethylene using metal oxide chemiresistors with a Pd-V<sub>2</sub>O<sub>5</sub>-TiO<sub>2</sub> yolk-shell catalytic overlayer via heterogeneous Wacker oxidation, *J. Mater. Chem. A* 11 (2023) 666–675.
- [107] R. Barthos, A. Hegyessy, G. Novodárszki, Z. Pászti, J. Vályon, Structure and activity of Pd/V<sub>2</sub>O<sub>5</sub>/TiO<sub>2</sub> catalysts in Wacker oxidation of ethylene, *Appl. Catal. A- Gen.* 531 (2017) 96–105.
- [108] P. Ivanov, E. Llobet, A. Vergara, M. Stankova, X. Vilanova, J. Hubalek, et al., Towards a micro-system for monitoring ethylene in warehouses, *Sens. Actuators B Chem.* 111–112 (2005) 63–70.
- [109] Y. Rotem, A. Wachs, D.R. Lewin, Ethylene compressor monitoring using model-based PCA, *AIChE J.* 46 (2000) 1825–1836.
- [110] E. Espinosa, R. Ionescu, S. Zampolli, I. Elmi, G.C. Cardinali, E. Abad, et al., Drop-coated sensing layers on ultra low power hotplates for an RFID flexible tag microlab, *Sens. Actuators B Chem.* 144 (2010) 462–466.
- [111] N.J. Pineau, J.F. Kompalla, A.T. Güntner, S.E. Pratsinis, Orthogonal gas sensor arrays by chemoresistive material design, *Microchim. Acta.* 185 (2018) 563.



**Cheyeon Kim** earned her B.S. in Advanced Materials Engineering from Jeonbuk National University in Korea, in 2023. She is currently pursuing an M.S. degree at Jeonbuk National University, focusing on ethylene-sensing materials for monitoring ethylene emissions from fresh produce.



**Ji-Wook Yoon** has been an Associate Professor in the Division of Advanced Materials Engineering at Jeonbuk National University since 2019. He earned his BS and MS/Ph.D. integrated degrees from Korea University in 2011 and 2017, respectively. He then worked as a research associate at ETH Zürich, Switzerland (2017–2018) and as a research professor at Korea University (2018–2019). His research focuses on the design and synthesis of oxide-based nanomaterials for use in chemical sensors, dielectrics, and batteries. For more information, please visit <http://sseljbnudothome.co.kr/>